



Vertical niche definition of test-bearing protists (Rhizaria) into the twilight zone revealed by in situ imaging

Tristan Biard, Mark D Ohman

► To cite this version:

Tristan Biard, Mark D Ohman. Vertical niche definition of test-bearing protists (Rhizaria) into the twilight zone revealed by in situ imaging. *Limnology and Oceanography*, 2020, 65 (11), pp.2583 - 2602. <10.1002/lno.11472>. <hal-03716825>

HAL Id: hal-03716825

<https://hal.science/hal-03716825v1>

Submitted on 7 Jul 2022

HAL is a multi-disciplinary open access archive for the deposit and dissemination of scientific research documents, whether they are published or not. The documents may come from teaching and research institutions in France or abroad, or from public or private research centers.

L'archive ouverte pluridisciplinaire **HAL**, est destinée au dépôt et à la diffusion de documents scientifiques de niveau recherche, publiés ou non, émanant des établissements d'enseignement et de recherche français ou étrangers, des laboratoires publics ou privés.



HAL Authorization



Vertical niche definition of test-bearing protists (Rhizaria) into the twilight zone revealed by in situ imaging

Tristan Biard, Mark D Ohman

► To cite this version:

Tristan Biard, Mark D Ohman. Vertical niche definition of test-bearing protists (Rhizaria) into the twilight zone revealed by in situ imaging. *Limnology and Oceanography*, Association for the Sciences of Limnology and Oceanography, 2020, 65, pp.2583 - 2602. 10.1002/lno.11472 . hal-03716825

HAL Id: hal-03716825



<https://hal.archives-ouvertes.fr/hal-03716825>

Submitted on 7 Jul 2022

HAL is a multi-disciplinary open access archive for the deposit and dissemination of scientific research documents, whether they are published or not. The documents may come from teaching and research institutions in France or abroad, or from public or private research centers.

L'archive ouverte pluridisciplinaire **HAL**, est destinée au dépôt et à la diffusion de documents scientifiques de niveau recherche, publiés ou non, émanant des établissements d'enseignement et de recherche français ou étrangers, des laboratoires publics ou privés.

Vertical niche definition of test-bearing protists (Rhizaria) into the twilight zone revealed by in situ imaging

Tristan Biard ^{1,2*} Mark D. Ohman ²

¹LOG, Laboratoire d'Océanologie et de Géosciences, Univ. Littoral Côte d'Opale, Univ. Lille, CNRS, UMR 8187, Wimereux, France

²Scripps Institution of Oceanography, University of California, San Diego, California

Abstract

The Rhizaria is a super-group of amoeboid protists with ubiquitous distributions, from the euphotic zone to the twilight zone and beyond. While rhizarians have been recently described as important contributors to both biogenic silica and carbon fluxes, we lack the most basic information about their ecological habitats and preferences. Here, using in situ imaging (Underwater Vision Profiler 5), we characterize the vertical ecological niches of different test-bearing pelagic rhizarian taxa in the southern *California Current Ecosystem*. We define three vertical layers between 0 and 500 m occupied, respectively, by (1) surface dwelling and mostly symbiont-bearing rhizarians (Acantharia and Collodaria), (2) flux-feeding phaeodarians in the lower epipelagic (100–200 m), and (3) Foraminifera and Phaeodaria populations adjacent to the oxygen minimum zone. We then use Generalized Additive Models to analyze the response of each rhizarian category to a suite of environmental variables. The models explain between 9% and 93% of the total variance observed for the different groups. While temperature and the depth of the deep chlorophyll maximum appear as the main abiotic factors influencing populations in the upper 200 m, dissolved silicon concentration is related to the abundance of mesopelagic phaeodarians, though it explains only a portion of the variance. The importance of biotic interactions (e.g., prey availability, predation, parasitism, symbiosis) is still to be considered, in order to fully incorporate the dynamics of test-bearing pelagic rhizarians in ecological and biogeochemical models.

Over the last two decades, interest has been elevated in the role of unicellular eukaryotes (i.e., protists) in marine global biogeochemical cycles (Worden et al. 2015). Among the large diversity of protists inhabiting the ocean (Massana 2015; Simpson et al. 2017), the Rhizaria is a diverse super-group of unicellular organisms, some of which have planktonic life styles (Burki and Keeling 2014). A characteristic feature of many marine rhizarians is the formation of a mineral test (or skeleton), whose chemical nature varies among taxa: Acantharia use strontium sulfate (SrSO_4), Polycystine radiolarians and Phaeodaria secrete opaline silica ($\text{SiO}_2 \cdot n\text{H}_2\text{O}$), and Foraminifera form calcium carbonate (CaCO_3) tests (Kimoto 2015; Nakamura and Suzuki 2015; Suzuki and Not 2015). With their mineralized skeletons eventually sinking upon death, test-bearing rhizarians actively contribute to fluxes of biogenic material into the deep ocean: Foraminifera are responsible for 32–80% of annual CaCO_3 export to the deep ocean (Erez 2003), Acantharia play a critical role in the

ocean's strontium budget (Bernstein et al. 1987), Polycystines/Phaeodaria can act as major exporters of biogenic silica (Biard et al. 2018) and Rhizaria altogether contribute to particulate organic carbon fluxes, especially in oligotrophic regions (Lampitt et al. 2009; Guidi et al. 2016; Stukel et al. 2018). Despite their active contribution to biogeochemical processes and substantial contribution to the marine carbon pool (Biard et al. 2016), there are still many critical gaps in our knowledge of test-bearing rhizarians, impeding full understanding of their ecological significance at local-to-global scales.

With fossil records as old as the lower Paleozoic (ca. 515 Ma), test-bearing rhizarians are among the oldest protist lineages found in modern oceans (Suzuki and Oba 2015). Through their long evolutionary history, they have adapted to a multitude of environmental conditions resulting in the ubiquity of contemporary rhizarians. They thrive from polar regions to warm equatorial waters, and from the sunlit surface to the dark meso- and bathypelagic ocean (Anderson 1983; Suzuki and Not 2015). A substantial fraction of test-bearing rhizarians inhabit the euphotic zone, hosting multiple photosymbionts from diverse eukaryotic and prokaryotic lineages (e.g., dinoflagellates, cyanobacteria; Anderson 2012; Decelle et al. 2015). This mixotrophic behavior allows some of them to thrive in environments such as oligotrophic gyres

*Correspondence: tristan.biard@univ-littoral.fr

Additional Supporting Information may be found in the online version of this article.

where food and nutrients are scarce (Taylor 1982; Biard et al. 2016). Deeper, in the dark ocean, are found deep-dwelling rhizarians (e.g., Phaeodaria; Nakamura and Suzuki 2015), with various trophic modes. Some are carnivores feeding on mesopelagic plankton (e.g., Foraminifera; Hull et al. 2011), or flux feeders (e.g., phaeodarians), feeding on carbon rich particles raining from the euphotic layer (Gowing 1989). To date, most of the limited knowledge on rhizarian distribution patterns—both horizontal and vertical—is still inferred from surficial sediment samples, and little information is available on taxon-specific vertical niche distribution in the water column (Kling and Boltovskoy 1995). In addition, as with many protistan lineages (Caron et al. 2004), test-bearing rhizarians remain mostly uncultured (with the exception of some planktonic foraminifera; Kimoto 2015). Therefore, in situ experiments and observations are currently the only reliable alternative (apart from DNA surveys, which lack a true quantitative dimension) to improve knowledge of rhizarian ecology and vertical niche distribution.

Numerous in situ imaging ocean systems are available (Benfield et al. 2007), with different advantages and drawbacks, and sampling characteristics, ranging from towed systems (e.g., Video Plankton Recorder—Davis et al. 1992a; In Situ Ichthyoplankton Imaging System—Cowen and Guigand 2008), vertical profilers (e.g., Underwater Vision Profiler; Picheral et al. 2010), to fully autonomous underwater vehicles (e.g., *Zooglider*; Ohman et al. 2018). Despite different technical specifications, in situ imaging approaches all share the same potential to study delicate organisms, including appendicularians and cnidarians (Luo et al. 2014; Greer et al. 2015; Ohman et al. 2018; Ohman 2019), colonial bacteria (Davis et al. 1992b) or test-bearing rhizarians (Dennett et al. 2002; Biard et al. 2016; Nakamura et al. 2017; Gaskell et al. 2019), which are typically severely disrupted by conventional sampling methods. In addition to unreliably sampling fragile organisms, even vertically stratified plankton nets (e.g., MOCNESS, MULTINET; Wiebe and Benfield 2003) fail to resolve the fine vertical distribution patterns of planktonic taxa. In contrast, towed and autonomous in situ imaging systems have successfully revealed fine-scale distribution patterns of zooplankton communities and the influence of environmental variables (Luo et al. 2014; Greer et al. 2015; Faillettaz et al. 2016; Ohman et al. 2018).

In the present study, we use the in situ imaging Underwater Vision Profiler 5 (UVP5) to identify large test-bearing rhizarians ($> 600 \mu\text{m}$; Biard et al. 2016) and characterize their ecological preferences and vertical niche distributions. We use in situ images collected during extensive vertical profiles on four research cruises of the *California Current Ecosystem* Long-Term Ecological Research (CCE-LTER) program (2008–2016; Ohman et al. 2013). CCE-LTER is situated in the southern California Current System, which encompasses a productive eastern boundary current coastal upwelling ecosystem and diverse other hydrographic regimes. Notably, the CCE region is characterized by a high diversity of test-bearing rhizarians (136–200 radiolarian species, mainly sampled from small size

fractions; Kling and Boltovskoy 1995) with periodically high abundances/biovolumes of larger cells ($> 600 \mu\text{m}$) that can represent a substantial fraction of zooplankton communities (Biard et al. 2016), as well as vertical fluxes of carbon (Stukel et al. 2018) and biogenic silica (Biard et al. 2018). Vertical profiling with the UVP5 was conducted from the euphotic region down to the dark mesopelagic ocean in order to define the ecological preferences of diverse test-bearing rhizarians. We also employ Generalized Additive Models to model the responses of rhizarian abundance to different environmental variables in relation to habitat depth and time.

Methods

In situ analysis of rhizarian populations

In situ measurements of rhizarian populations were acquired between 2008 and 2016 on four process cruises of the *California Current Ecosystem* Long-Term Ecological Research (CCE-LTER) Program (P0810, P1208, P1408, P1604; the first two digits designate the year and the second two the month). While the different process cruises were directed to specific questions (Ohman 2018), they all shared the same quasi-Lagrangian design, whereby water parcels of interest (labeled as a “Cycle”) were sampled intensively while following the same planktonic population for several days (2–5 d; Landry et al. 2009; Ohman et al. 2013). During these Lagrangian experiments, covering a wide range of hydrographic conditions (e.g., coastal upwelling, mesotrophic waters, offshore oligotrophic waters; details in Stukel et al. 2018), we conducted repeated vertical profiles (between 5 and 16, but typically 10 in each water parcel) with a CTD-rosette equipped with the in situ imaging system UVP5. The UVP5 is designed to quantify particle concentrations and image large planktonic organisms ($> 600 \mu\text{m}$) at fine vertical scales ($\sim 1 \text{ L image}^{-1}$, 5–20 cm vertical sampling resolution; Picheral et al. 2010). Although the dimensions of an individual pixel are $\sim 150 \mu\text{m}$, we consider a minimum grid of 4×4 pixels as necessary to resolve an individual organism, hence we refer to a detection limit of $600 \mu\text{m}$. Here, the smallest rhizarian identified had an equivalent spherical diameter (ESD) of $877 \mu\text{m}$. In the present study, abundance data were binned in depth intervals of 5 m, while discrete depth was considered for individual vignettes. A total of 205 vertical UVP5 profiles were retained to estimate integrated abundances, vertical distribution and ecological niche of test-bearing rhizarians (Fig. S1). Only 154 of these vertical profiles extended to 500 m (i.e., upper mesopelagic). These vertical profiles (median sampled volume of 6 m^3 for a 500 m deep profile) generated 22,504 individual rhizarian vignettes (i.e., individual image of organisms $> 600 \mu\text{m}$), after processing the raw images as described in Biard et al. (2016, 2018). All images were manually identified and classified by a single experienced person (T.B.). Taxonomic classifications follow Adl et al. (2019) and Nakamura and Suzuki (2015). Upon request, all individual vignettes, their associated morphometric measures

(e.g., area, ESD, etc.) and binned abundances are accessible online at Ecotaxa (<http://ecotaxa.obs-vlfr.fr>; Picheral 2017).

Identification of in situ images of Rhizaria

Rhizarian images were first separated into different morphotypes based on common morphological features (e.g., overall shape, presence of spines, etc.) and then further assigned to taxonomic groups (Fig. 1) based on comparisons with a collection of rhizarian specimens collected in regional waters and elsewhere (Fig. 2), as well as previous in situ imaging studies on Rhizaria (Biard et al. 2016; Nakamura et al. 2017). Given the UVP5 resolution (see above), morphological criteria are limited for the smaller end (i.e., 600–1000 μm) of rhizarians detectable with this device and taxonomic assignments could include errors. However, we briefly summarize below the key criteria needed to reproduce the present delineation and present the potential points of confusion between groups. We also refer the reader to our Data S1, which contains a detailed guide used to discriminate the different categories:

Collodaria: large specimens either found as colonies (elongated shape with multiple dots) or solitary specimens (large sphere with a dark nucleus) as shown previously in Biard et al. (2016) by direct comparison with light microscopy. *Possible confusion* with Castanellidae, but solitary Collodaria display a larger halo with a gradient of gray surrounding the nucleus.

Acantharia: specimens of variable sizes, all displaying a symmetrical star-shape. *Possible confusion* with some Aulacanthidae, but the latter lack this symmetry.

Castanellidae: spheres with a dark central sphere (malacoma + scleracoma) from which arise tiny projections (i.e., spines). The entire central sphere is surrounded by an extended network of ectoplasm (gray halo). The extent of the halo is constant (i.e., diameter of nucleus = 1/3 of the sphere diameter). *Possible confusion* with solitary Collodaria, but for the halo diameter and gradient of gray noted above.

Aulosphaeridae: sphere with a dark gray nucleus (phaeodium) in its center, a geometric meshwork (skeleton) and numerous short spines often visible at the periphery, as shown previously in Biard et al. (2016) by direct comparison with light microscopy.

Medusettidae: specimens with ovoid central part from which three pairs of long branch-like extensions (styles) arise. *Possible confusion* with some Coelodendridae, Aulacanthidae, or Acantharia, but none of those taxa possess these pairs of extensions.

Foraminifera: specimens with extended network of filaments (pseudopods) reaching up to 10 times the length of the central test.

Aulacanthidae: specimens with variable shapes, often spherical/ovoid with a phaeodium in its center and a variable number of peripheral spines. *Possible confusion* with Acantharia, Medusettidae, or Aulosphaeridae, but the latter lack the medium-sized peripheral spines.

Coelodendridae: specimens ranging from arrow-like shapes to ovoid cells with medium-to-large branch-like extensions (styles). *Possible confusion* with Medusettidae, apart from the extensions noted above.

Cannosphaeridae: large specimens with a loosely constructed geometric meshwork (skeleton) and a small phaeodium in the center. *Possible confusion* with Aulosphaeridae, but the latter have a denser meshwork.

Phaeodaria (*Circoporidae*?): specimens with an angular cell with 11–14 long spines emerging from the center.

Tuscaroridae: large colonial specimens with a dozen individual cells displaying 2–3 spicules oriented to the outside, and attached to a large spherical or intricate central structure.

Context of this study with respect to previous research

The present study uses an extensive dataset of in situ images, most of which have not been used in any published work. A portion of this dataset (from only the 2008 cruise), with coarse taxonomic resolution (i.e., only Acantharia, Collodaria, Phaeodaria, and other Rhizaria were considered), was incorporated in a worldwide study of plankton patterns (Biard et al. 2016). A second subset (images of the single family Aulosphaeridae recorded in 2008, 2012, 2014, and 2016) was used for analyses of rhizarian-mediated fluxes (Biard et al. 2018; Stukel et al. 2018). In contrast, the present study uses all available rhizarian in situ images in an original analysis of the ecological preferences of the complete suite of 12 taxonomic groups over vertical gradients spanning the sea surface to 500 m depth, in a specific Eastern Boundary Current ecosystem.

Environmental data

To assess the influence of environmental variables on rhizarian distributions, we created a matrix of abiotic variables obtained from (1) CTD downcast data and (2) water-column dissolved inorganic nutrients, sampled at discrete depths. Data, along with detailed sampling and analytical methods, can be found at <http://oceaninformatics.ucsd.edu/datazoo/catalogs/ccelter/datasets>. From this matrix of environmental data, we used six variables: temperature ($^{\circ}\text{C}$); dissolved oxygen concentration ($\mu\text{mol kg}^{-1}$); Chl *a* concentration ($\mu\text{g L}^{-1}$); depth of the deep chlorophyll maximum, DCM (m); Chl *a* concentration at the DCM ($\mu\text{g L}^{-1}$); and dissolved silicon (dSi) concentration ($\mu\text{mol L}^{-1}$). Temperature was measured using recently calibrated Seabird sensors (SBE 3). Dissolved oxygen was measured using a calibrated SBE 43 polarographic membrane sensor. Chl *a* (<http://www.calcofi.org/ccpublications/calcofi-methods/8-chlorophyll-methods.html>) and dSi concentrations (<http://www.calcofi.org/ccpublications/calcofi-methods/422-nutrient-methods.html>) were measured on water samples collected at discrete depths with Niskin bottles. Dissolved silicon concentrations were linearly interpolated (0–500 m) from discrete measurement for each Lagrangian Cycle. Depth of the DCM was determined as the maximum value of in vivo Chl *a* fluorescence detected by the

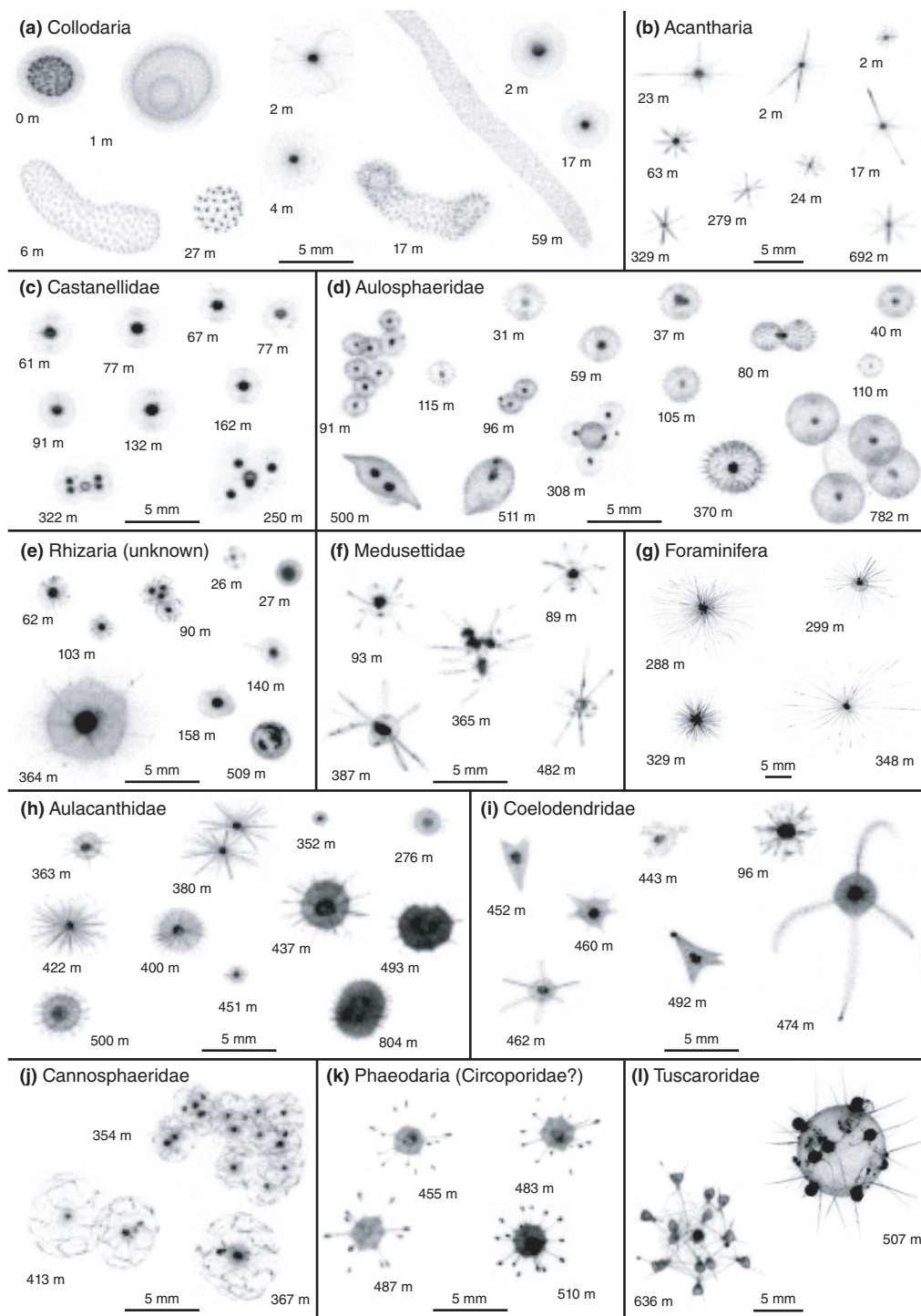


Fig. 1. Diversity of representative test-bearing rhizarians obtained with the UVP5 in the *California Current Ecosystem*. **(a)** Collodaria, **(b)** Acantharia, **(c)** Castanellidae, **(d)** Aulosphaeridae, **(e)** Rhizaria unknown, **(f)** Medusettidae, **(g)** Foraminifera, **(h)** Aulacanthidae, **(i)** Coelodendridae, **(j)** Cannosphaeridae, **(k)** Phaeodaria (Circoporidae?), and **(l)** Tuscaroridae. Each vignette is displayed with the depth where the organism was observed. All images are scaled the same, except for the Foraminifera and Tuscaroridae.

fluorometer attached to the CTD rosette (after a smoothed moving average). Particle (0.20–27 mm) concentrations were recorded in situ by the UVP5.

For each taxonomic group, determined based on common morphological characteristics (*see* Results and the taxonomic guide in Data S1), we considered the central vertical niche as

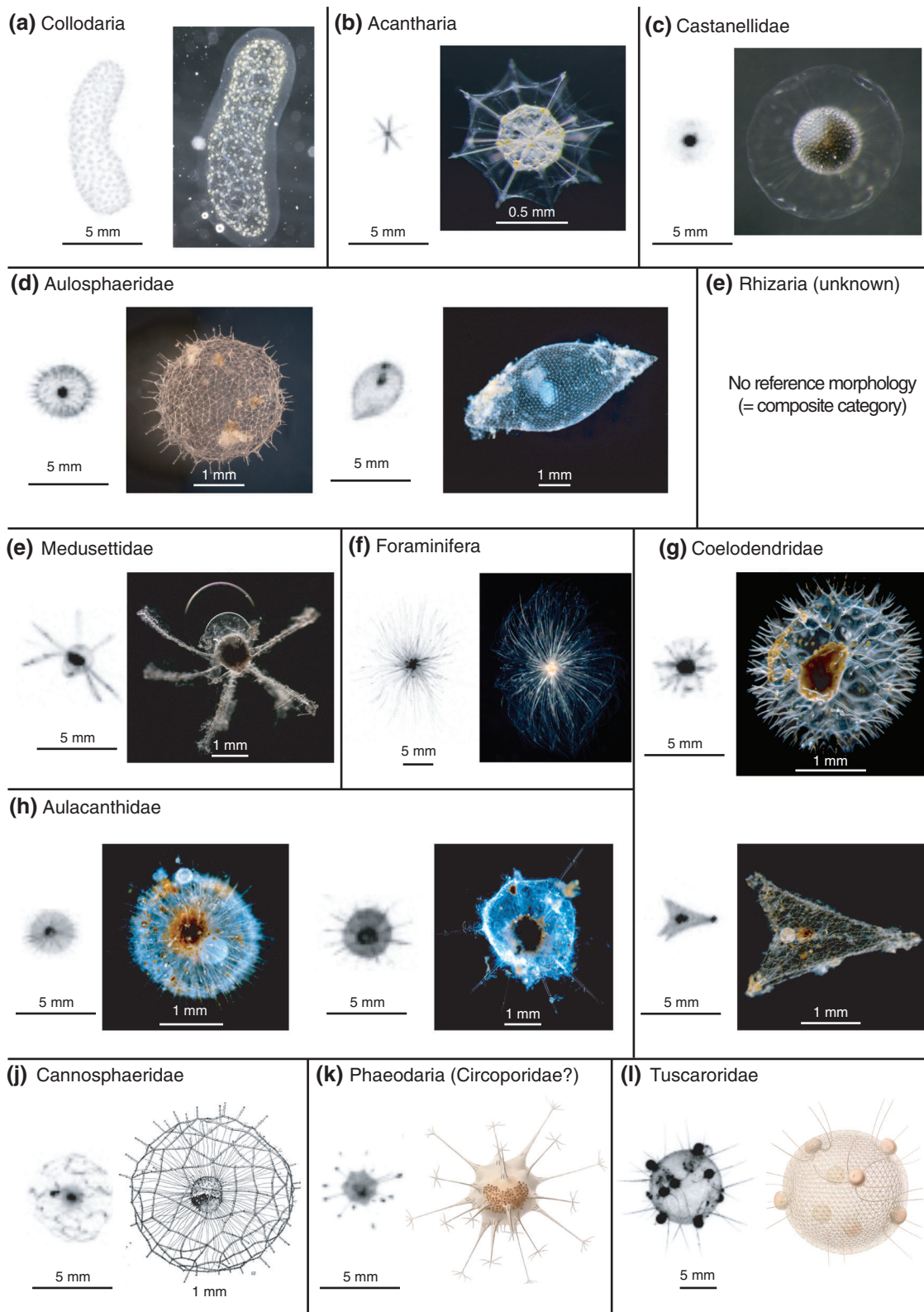


Fig. 2. Comparison between UVP5 images and light microscope images (or illustrations from published monographs) for our different taxonomic categories. None of these comparisons were made with the same specimens, as previously published (Biard et al. 2016). However, specimens from **(a)**, **(d)**, **(e)**, **(f)** Medusettidae, **(g)** Foraminifera, **(h)** Aulacanthidae, and **(i)** Coelodendridae were collected in the same CCE water as UVP5 images. Monographs of Cannosphaeridae from Reshetnyak (1955) and Circoporidae/Tuscaroridae from Haecker (1908). Images **(b)** courtesy of Dr. Shinji Shimode (Yokohama National University), **(c)** courtesy of Dr. Katsunori Kimoto (JAMSTEC), and **(f)** courtesy of Linda Lanniello (Blackwater Creatures).

the median depth (\pm interquartile range) where corresponding vignettes were observed. Subsequently, for these central vertical niches, we computed a mean value for each abiotic variable retained (see above).

Statistical analysis

All data analysis was conducted using R 3.4.4. (R Core Team, 2018), custom scripts and the following packages: *tidyverse* (Wickham and RStudio 2017) and *visreg* (Breheny and Burchett 2017). Nonparametric rank correlation tests (Kendall's Tau; Kendall and Gibbons 1990) were used to investigate relationships between: (1) rhizarian cell sizes and depth, and (2) chlorophyll *a* concentration at the DCM and the depth of the DCM (see Section 2). For each test we reported Kendall's Tau (correlation coefficient) and *p* value (test significance).

We used Generalized Additive Models (GAMs; Hastie and Tibshirani 1986; Guisan et al. 2002; Wood 2017) implemented in R package *mgcv*, to model the relationship between the abundance of different taxonomic groups of test-bearing rhizarians (log-transformed) and a set of environmental variables. GAMs are non-parametric extensions of Generalized Linear Models that offer a powerful and flexible alternative that can estimate both linear trends as well as non-monotonic responses, which is particularly helpful for describing ecological patterns. The parameter controlling the degree of smoothness was reduced ($k = 5$) to avoid over-smoothing of the data. For each taxonomic group, analyses of their responses to environmental variables were constructed based on the following rationale:

1. A subset of environmental variables was first selected a priori, based on hypotheses found in literature. For example, only taxonomic groups including siliceous skeleton-bearing rhizarians were tested against dissolved silicon concentrations, or only potential flux-feeders were tested against particle concentrations.
2. A GAM was first performed with the inclusion of year (i.e., cruise) as predictor to account for interannual (inter-cruise) variations. The GAM was formulated as $\text{Log}(\text{Abundance}) \sim s(\text{Variable } 1) + s(\text{Variable } n) + \text{cruise}$, where *s* represents the smoothing function for the different *n* variables. If significant, we reported the responses of each smoothed term on a yearly basis (see Table S1).
3. If no statistically significant effect of cruise was determined, we removed the year as a predictor variable and performed a second GAM (using the same equation as shown above, without cruise). For each model, we obtained the following metrics: fitted values, residuals, adjusted R^2 , restricted maximum likelihood (REML) score, deviance explained (%), and *p* values for *F* statistics. We report the last four values in Table S1. For each GAM output, we provide a smoothed spline (reduced to a simple linear effect if necessary) of each

variable's relative contribution to predicting observed abundances, as well as an overall model.

Results

Diversity of test-bearing rhizarians

Twelve distinct categories of large rhizarians (i.e., $> 600 \mu\text{m}$) were delineated based on common morphological features (see Data S1 for the detailed morphological criteria used to discriminate the different categories) and assigned to the following taxonomic groups: two types of radiolarians, one foraminiferan, and eight phaeodarians (Figs. 1, 2). A subset of vignettes ($n = 188$) could not be clearly assigned to one of the other 11 specific rhizarian categories and were, in this case, assigned to a general category (Fig. 1e). These categories are hereafter described starting with those inhabiting surface waters, continuing with those dwelling deeper.

Collodaria (Figs. 1a, 2a), comprising both colonial and solitary forms ($n = 487$ vignettes), and Acantharia (Figs. 1b, 2b) ($n = 931$) occur mainly in the upper epipelagic zone (< 100 m). At the base of the euphotic zone (~ 100 m), two phaeodarian families were identified: Castanellidae ($n = 814$; Figs. 1c, 2c) and numerous specimens of Aulosphaeridae ($n = 18,772$; Figs. 1d, 2d). At greater depths, the phaeodarian family Medusettidae ($n = 30$) was represented by a few organisms (Figs. 1f, 2f) and occurred along with Foraminifera ($n = 196$; Figs. 1g, 2g), and the phaeodarians Aulacanthidae ($n = 725$; Figs. 1h, 2h) and Coelodendridae ($n = 271$; Figs. 1i, 2i). The three remaining phaeodarian categories were restricted to waters deeper than 350 m: the Cannosphaeridae ($n = 33$; Figs. 1j, 2j), a group of phaeodarians, likely belonging to the family Circoporidae ($n = 61$; Figs. 1k, 2k) and three specimens members of the family Tuscaroridae (Figs. 1l, 2l).

Overall, test-bearing rhizarians detectable by UVP5 encompassed organisms ranging in size (expressed as ESD) from $877 \mu\text{m}$, for a single cell of Castanellidae, to 12.6 mm for a colonial collodarian (Fig. 3). We observed a significant tendency of increasing size of rhizarians with increasing depth (Kendall's $T = 0.24$; $p < 0.05$). While most categories included organisms with diameters between 1 and 3 mm, several taxa including the Foraminifera, Tuscaroridae, and Cannosphaeridae, mostly exceed a mean size of 3 mm. These three taxa, in addition to colonial collodarians, included organisms of large individual sizes (e.g., Cannosphaeridae), with extended pseudopodial webs (e.g., Foraminifera) or those forming large colonies (e.g., Tuscaroridae). We observed that not only the preceding taxa, but all phaeodarian families can often occur as colonies of several unicellular specimens. This colonial feature explains some of the size variability within a single taxon (e.g., Aulosphaeridae; Figs. 1, 3).

Vertical niche definition

In order to define test-bearing rhizarians' realized ecological niches, we compared their vertical distribution with profiles of environmental variables, including temperature, dissolved silicon and dissolved oxygen (Fig. 3). We defined three layers

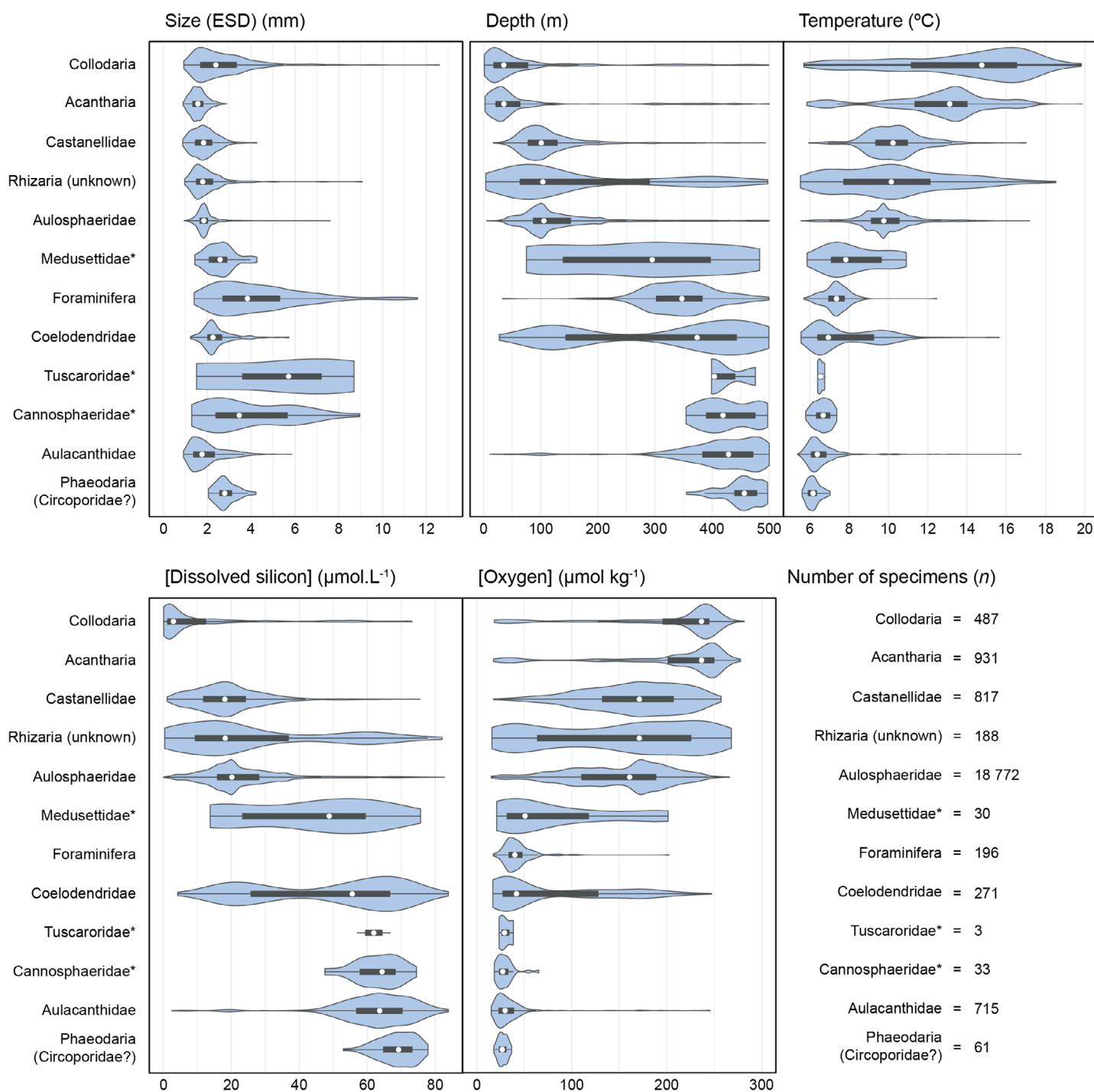


Fig. 3. Niche definition of test-bearing rhizarians. Violin plots showing the size distribution and affinity of different rhizarian taxa with four environmental variables. Boxplot indicates median (white dot), ranges between the first and third quartiles, and whiskers cover extreme data points within 1.5 IQR range from the quartiles. Blue areas are kernel density plots (represented symmetrically on both sides) showing the probability density distributions of the data. Number of specimens in each category is displayed in the bottom right panel. Acantharia and Foraminifera are omitted from the dissolved silicon plot because they are not known to utilize it.

occupied by specific taxa (Fig. 4a) and observed an overall increase of morphotype diversity in the epipelagic and the upper mesopelagic (Fig. 4b).

The upper ocean or epipelagic zone was characterized by the presence of Collodaria (median vertical niche = 35 m) and

Acantharia (35 m), found primarily in the first 100 m (but sporadically down to 500 m). These two taxa occurred at temperatures ranging from > 11°C to 14–16°C, for Acantharia and Collodaria, respectively, and thrived in well oxygenated and dissolved silicon-depleted surface waters.

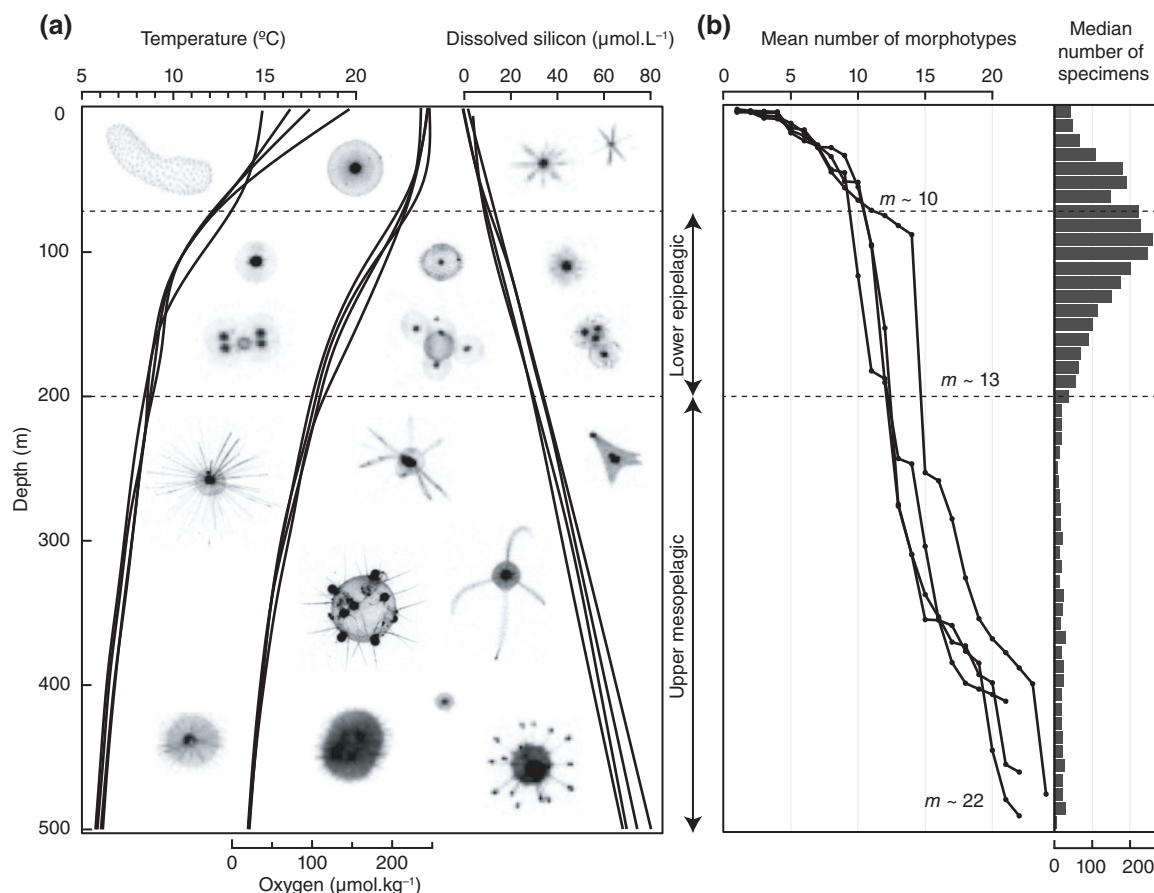


Fig. 4. Vertical niche zonation of test-bearing protists (Rhizaria) into the twilight zone of the *California Current Ecosystem*. **(a)** Average vertical profiles (four lines, one for each cruise) of temperature (left), oxygen concentration (middle) and dissolved silicon concentration (right) are displayed alongside representative rhizarian taxa. **(b)** Vertical distribution of rhizarian taxon richness (expressed as mean numbers of individual morphotypes) and rhizarian specimens (i.e., individual UVP5 vignette; expressed as the median number of specimens for a 10 m bin across the four different cruises). Numbers (m) at the bottom of each zone represent the average cumulative number of morphotypes.

At the base of the euphotic zone, in the lower epipelagic, we observed three taxa, the Castanellidae (101 m), the unknown Rhizaria (103 m) and finally the Aulosphaeridae (106 m). The three categories were mainly found in well oxygenated ($> 100 \mu\text{mol kg}^{-1}$) water, with temperatures of $10 \pm 1^\circ\text{C}$ and dissolved silicon concentrations of $\sim 20 \mu\text{mol L}^{-1}$.

The third vertical layer, corresponding to the upper mesopelagic (200–500 m), was characterized by a more diverse community (seven groups) of test-bearing rhizarians associated with colder temperatures ($< 8^\circ\text{C}$). Two taxa were transitional between the limit of the euphotic zone and the upper mesopelagic: Medusettidae were observed consistently between 150 and 400 m, while the Coelodendridae displayed a bimodal vertical distribution with higher densities at ~ 100 and ~ 400 m. Apart from these two specific taxa, the remaining ones (i.e., Foraminifera, Tuscaroridae, Cannosphaeridae, Aulacanthidae, and the likely Circoporidae), were associated with deep (> 300 m) mesopelagic waters, enriched in dissolved silicon ($> 60 \mu\text{mol L}^{-1}$) and close to the oxygen minimum zone (OMZ; oxygen concentration $< 50 \mu\text{mol kg}^{-1}$).

Rhizaria abundance over time

Integrated abundances of the different rhizarian categories (with the exception of the Tuscaroridae, which were too rare to be reliably sampled) were quantified in the different Lagrangian cycles and frontal studies (Fig. 5; Table S2). Considering all four cruises, Aulosphaeridae phaeodarians (Fig. 5d) were the most abundant test-bearing rhizarian taxon within the first 300 m (but also extending to 0–500 m). In the upper 300 m, the remaining taxa, Collodaria (Fig. 5a), Acantharia (Fig. 5b), and Castanellidae (Fig. 5c) showed integrated abundances of the same order of magnitude as one another. When extending to the mesopelagic (0–500 m), abundances of phaeodarians (Fig. 5e–l) and foraminifera (Fig. 5i) were also of the same order of magnitude, with the phaeodarian Aulacanthidae consistently being the most abundant overall.

The variability over time (i.e., within and between cruises) differed markedly among different types of test-bearing rhizarians and appeared slightly more pronounced in the upper ocean layer. Indeed, for Castanellidae and

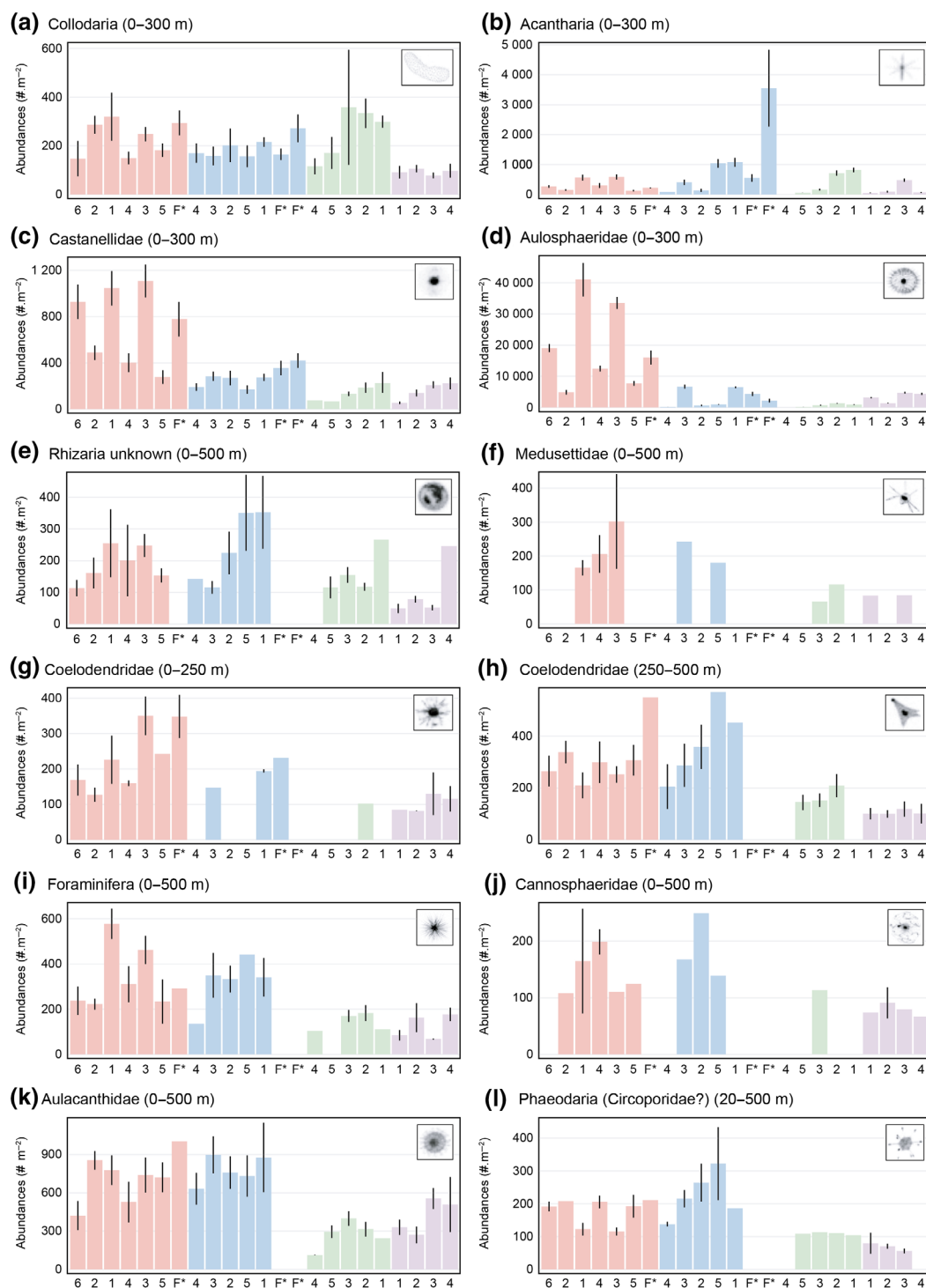


Fig. 5. Variation of rhizarian integrated abundances over the four process cruises (red: 2008; blue: 2012; green: 2014; purple: 2016). **(a)** Collodaria, **(b)** Acantharia, **(c)** Castanellidae, **(d)** Aulosphaeridae, **(e)** Rhizaria unknown, **(f)** Medusettidae, **(g,h)** Coelodendridae, **(i)** Foraminifera, **(j)** Cannosphaeridae, **(k)** Aulacanthidae, **(l)** Phaeodaria (Circoporidae?). Depth of integration is displayed in panel headers. Error bars denote standard error of the mean for each Lagrangian cycle (number along x-axis) or frontal studies (F* along x-axis). Within each year, Lagrangian Cycles are ordered from left to right along a gradient of increasing primary production (frontal studies are not ordered accordingly). Note the different y-axis scaling for each panel. Detailed values in Table S1.

Aulosphaeridae (Fig. 5c,d), abundances were considerably higher and more variable during the 2008 cruise (late summer/early fall) than for the three following years (spring and

summer cruises). For other taxa primarily occupying upper ocean layers (Collodaria and Acantharia; Fig. 5a,b), inter- and intra-cruise variability appeared reduced with

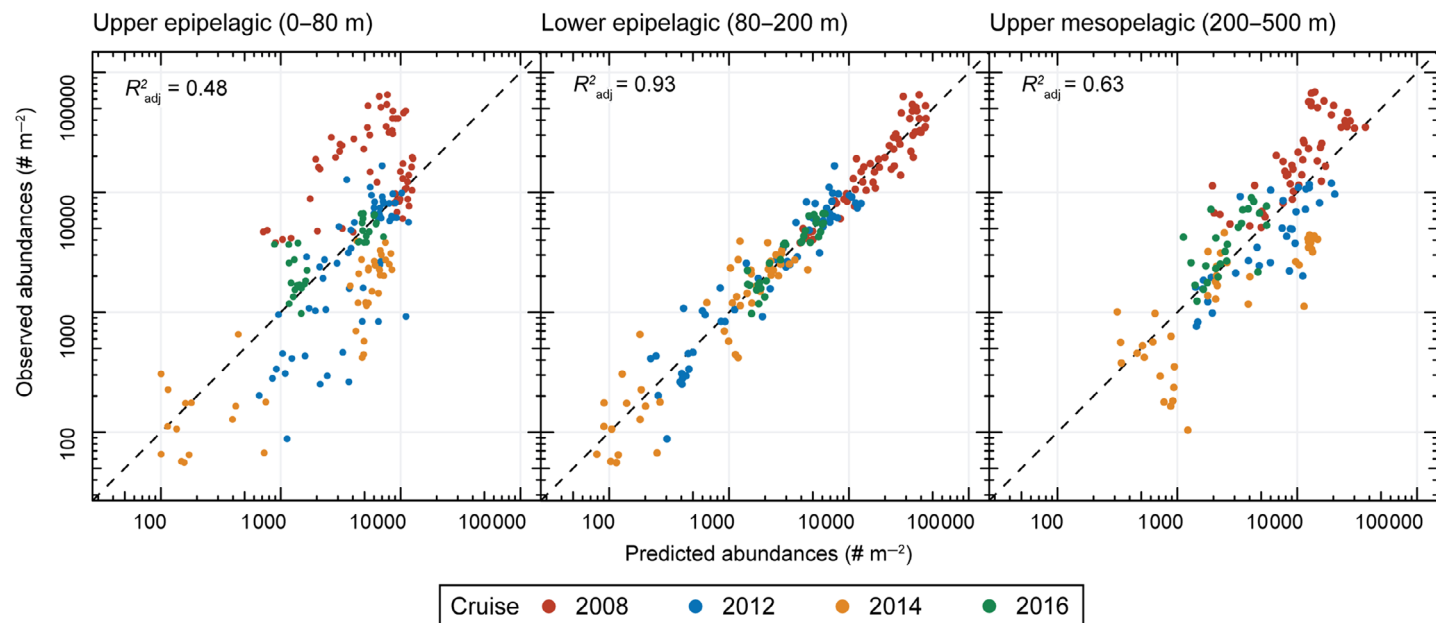


Fig. 6. GAMs based on selected niche abiotic characteristics of composite rhizarian populations in three vertical layers. Adjusted R^2 for the models is indicated for each vertical layer.

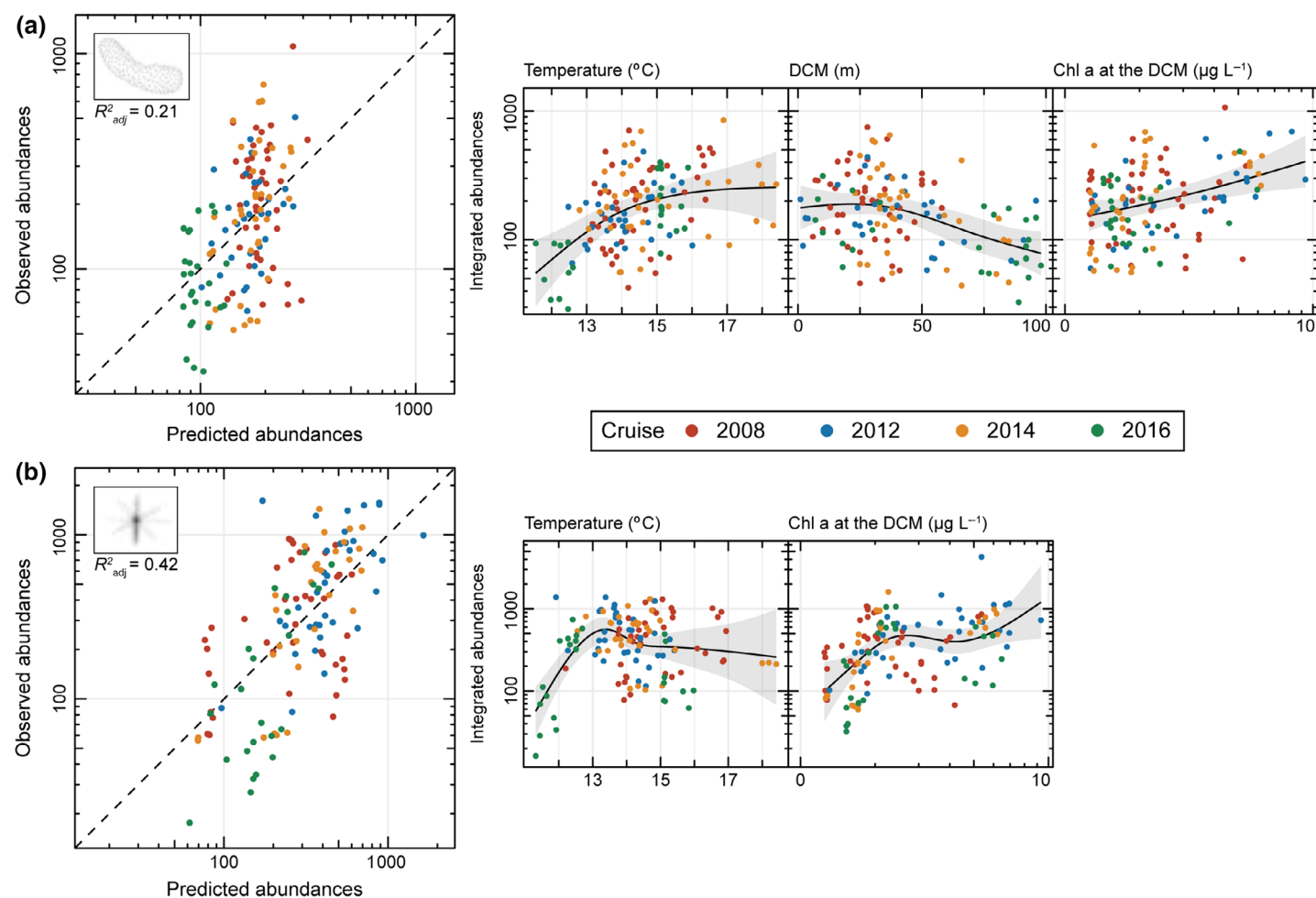


Fig. 7. GAMs based on selected niche abiotic characteristics of epipelagic rhizarians: (a) Collodaria and (b) Acantharia. Gray intervals denote the 95% confidence intervals for each spline. Adjusted R^2 for the models are indicated for each taxon.

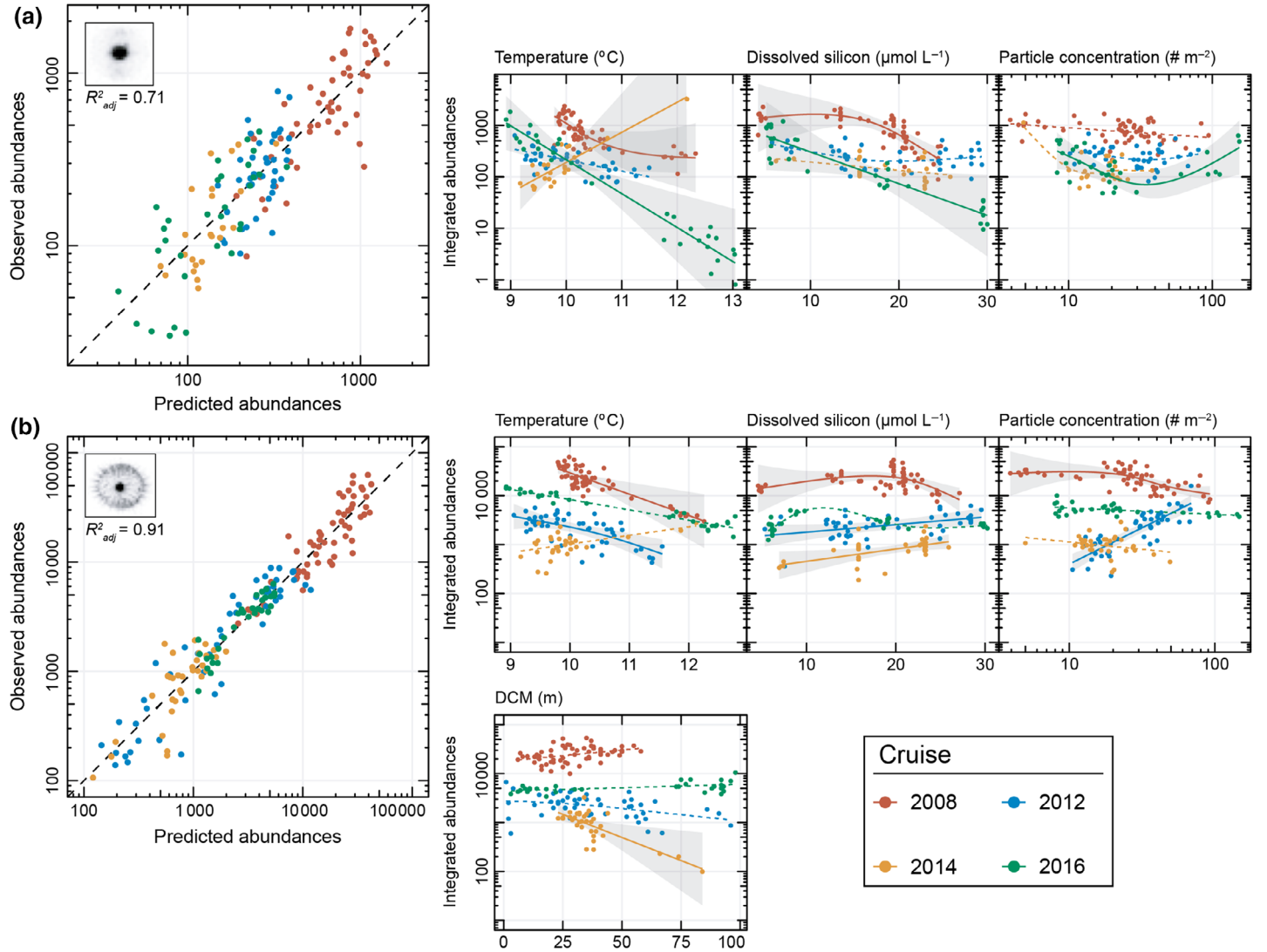


Fig. 8. GAMs based on selected niche abiotic characteristics of lower epipelagic rhizarians: **(a)** Castanellidae and **(b)** Aulosphaeridae. For subpanels, solid lines represent significant GAMs and dashed lines, insignificant GAMs. Gray intervals denote the 95% confidence intervals for each spline. Adjusted R^2 for the models are indicated for each taxon.

occasionally higher abundances in specific samples. Although we observed a diminution in integrated abundances between the 2008 + 2012 and the 2014 + 2016 cruises, this difference applied to almost all taxa, including those dwelling near the surface.

Influence of environmental variables on rhizarian populations

Having established the vertical niches of test-bearing rhizarians and their variability in abundance among cruises, we explored environmental variables that may explain and predict this variability. For each layer defined above, we first developed GAMs including all rhizarians, regardless of taxonomic affiliation (Figs. 6, S2). For the upper epipelagic zone

($R^2_{\text{adj}} = 0.48$, deviance explained = 51%), the depth of the DCM, Chl *a* concentration [Chl *a*] at the DCM and DCM depth were retained as explanatory variables. Deeper in the lower epipelagic, temperature, DCM, particle concentration and dissolved silicon were found to have significant effects on rhizarian abundances ($R^2_{\text{adj}} = 0.93$, deviance explained = 94%). A significant effect of sampling year was found. Finally, in the upper mesopelagic zone ($R^2_{\text{adj}} = 0.63$, deviance explained = 65%), rhizarian abundances were significantly influenced mainly by dissolved silicon followed by oxygen concentration, and to a lesser extent by temperature and particle concentration.

Next, in order to better understand the variables governing specific taxa, GAMs were fitted to the different rhizarian categories described above (Figs. 7–9), with the exception of

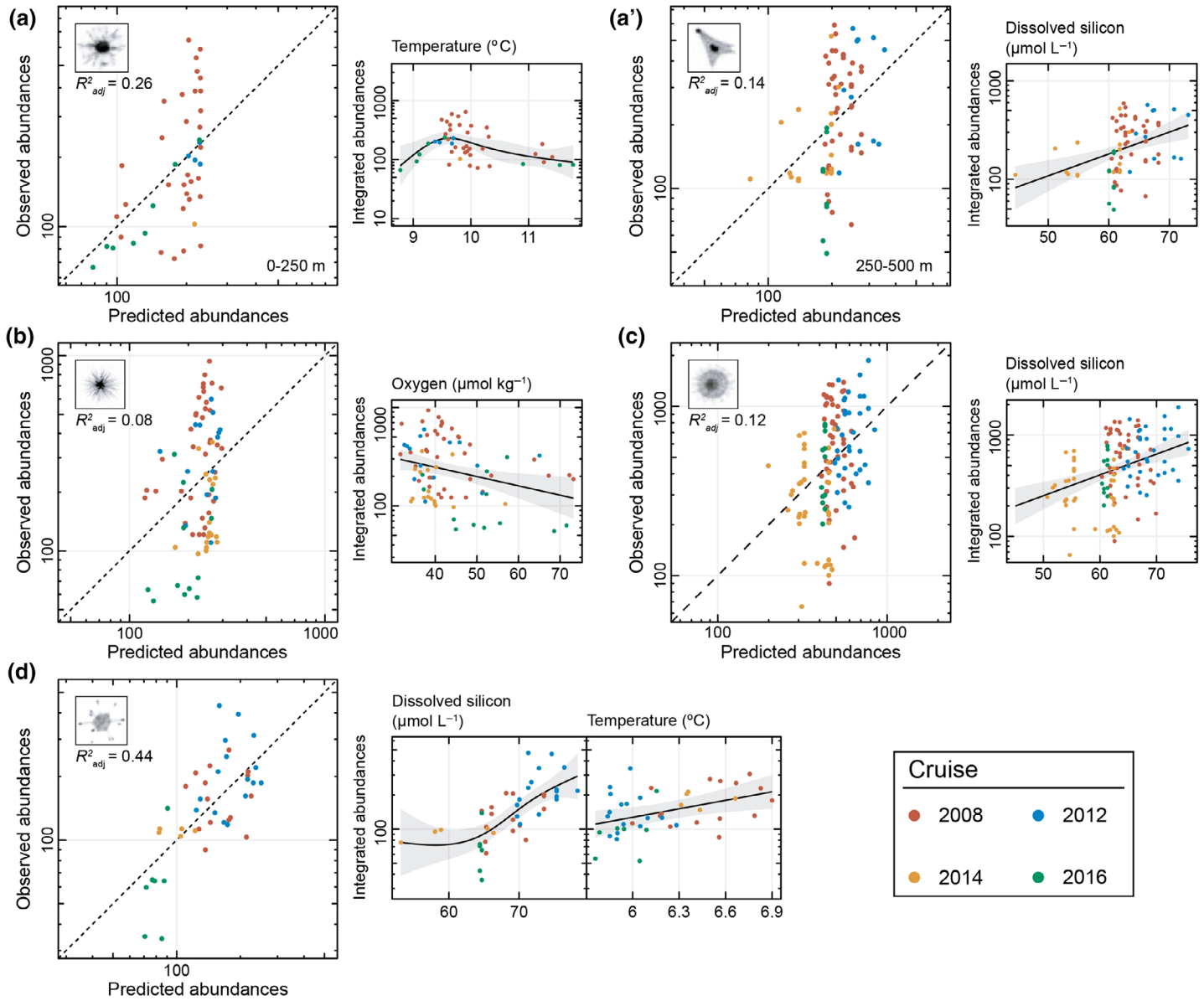


Fig. 9. GAMs based on selected niche characteristics of mesopelagic rhizarians: **(a-a')** Coelodendridae for a depth range of 0–250 m (left panels) and 250–500 m (right panels), **(b)** Foraminifera, **(c)** Aulacanthidae, and **(d)** Phaeodaria (Circoporidae?). Gray intervals denote the 95% confidence intervals for each spline. Adjusted R^2 for the models are indicated for each taxon.

Cannosphaeridae, Tuscaroridae, and Medusettidae, all of which were too rare to produce interpretable GAMs. Given the composite nature of “Rhizaria unknown,” no GAM was attempted for this category. Overall, statistical performances of GAMs differed substantially among the various groups (Table S1) but the same explanatory variables found to be significant in the GAMs performed by vertical layer (Figs. 6, S2), irrespective of taxonomic identity, were observed to have mostly the same influence for individual taxa.

Within the epipelagic zone, temperature, the depth of DCM and [Chl a] at the DCM were retained as explanatory variables for the GAMs, and produced R^2_{adj} of 0.42 and 0.21, for

Acantharia and Collodaria, respectively (Fig. 7; Table S1). No significant effect of sampling year was recorded for either taxon. For Collodaria, all three tested variables had significant effects (Fig. 7a), while the DCM depth appeared to have an insignificant effect in the model for Acantharia (Fig. 7b). The response to increasing temperatures revealed a positive response from 11 $^{\circ}\text{C}$ to 13–14 $^{\circ}\text{C}$ with increasing abundances of both taxa, followed by a reduced or negligible response (i.e., threshold effect). Both taxa showed the same response of increasing abundances with increasing [Chl a] at the DCM, while only Collodaria displayed a significant negative response to the deepening of the chlorophyll maximum (Fig. 7a).

For rhizarians dwelling in the lower epipelagic zone, temperature, DCM, particle concentration and dissolved silicon were explanatory variables. Carbon fluxes (recorded with sediment traps at 100 m) show no significant effects on abundances of both types of organisms (Castanellidae, Kendall's $T = 0.03$, $p = 0.60$, $n = 129$; Aulosphaeridae, $T = 0.07$, $p = 0.25$, $n = 150$) and were not considered further. The resulting GAMs produced moderate to strong R^2_{adj} values of 0.71 and 0.91 (detailed statistics shown in Table S1), for Castanellidae (Fig. 8a) and Aulosphaeridae (Fig. 8b), respectively. Here, year/cruise had a significant ($p_{2008,2012,2014,2016} < 0.001$ for both taxa) and strong effect on observed abundances. The contribution of each variable was non-uniform and produced different patterns for individual taxa, with the year 2014 (a time of exceptional warm anomalies; Zaba and Rudnick 2016) standing out with often opposite patterns. The resulting, yet contrasting models suggested: a general decrease in abundance with increasing temperature (except for 2014); a minimal effect of the DCM on both taxa; a limited effect of increasing particle concentration, except for the sharp increase of abundance of Aulosphaeridae in 2012. The modeled responses to increasing dissolved silicon concentration differed between Castanellidae and Aulosphaeridae, with the former showing a negative or negligible response, while the latter showed a weakly positive response.

In the third zone, i.e., the upper mesopelagic layer, GAMs produced models with low-to-moderate R^2_{adj} : < 0.26 for Foraminifera, Aulacanthidae, and Coelodendridae, and 0.44 for the unknown phaeodarians (Fig. 9; Table S1). Similar to the epipelagic GAMs, we detected no significant effects of sampling year on observed abundances of these four taxa, nor considered Carbon flux at 100 m as an explanatory variable. Although the overall GAM fits explained limited variance ($0.12 < R^2_{\text{adj}} < 0.26$), the three phaeodarian taxa from this upper mesopelagic layer consistently showed increased abundances with higher dissolved silicon concentration (Fig. 9a,c,d). The overall GAM model for Foraminifera explained little variance, but revealed a significant response of decreased abundances in increasing dissolved oxygen concentrations (Fig. 9b).

Discussion

Diversity of test-bearing rhizarians from in situ imaging

In situ images of test-bearing rhizarians in the *California Current Ecosystem* revealed 12 visually-recognizable morphological categories, with mixed taxonomic ranks inherent to the minimum size resolvable by the UVP5 ($> 600 \mu\text{m}$). Compared to the 12 morphotypes observed here, early studies in the CCE and nearby regions reported radiolarian diversity an order of magnitude higher, ranging from 136 to 200 species (Casey 1966; Boltovskoy and Riedel 1987; Kling and Boltovskoy 1995). These estimates of diversity cannot be directly compared with the present results, as early studies used plankton nets (with mesh size $\leq 62 \mu\text{m}$) targeting the small polycystines (e.g., Spumellaria, Nassellaria, etc.) that are

undetectable with the UVP5, and also analyzed preserved specimens by microscopy. However, since rhizarian tests can be easily damaged upon collection with plankton nets (Nakamura and Suzuki 2015; Suzuki and Not 2015) or dissolved upon preservation with traditional fixatives (Beers and Stewart 1970), in situ imaging confers other advantages. In situ imaging is a non-invasive means of observing fragile planktonic organisms (e.g., Remsen et al. 2004; Benfield et al. 2007), including test-bearing rhizarians, in their natural habitat. Such images can record natural feeding postures and extension of rhizopodia, the organisms' 3-dimensional orientation, aggregations of multiple cells, etc. (Dennett et al. 2002; Biard et al. 2016; Ohman et al. 2018; Gaskell et al. 2019). For non-rhizarian taxa, imaging has even resolved interactions between predators and prey (Ohman et al. 2018) and fine-scale distributions (Luo et al. 2014; Faillettaz et al. 2016).

While seven of the rhizarian categories observed here were previously described in this region, others, including the phaeodarians Medusettidae, Coelodendridae, Cannosphaeridae, and Tuscaroridae have rarely been reported in the CCE, and in few instances worldwide. Among these taxa, Cannosphaeridae are often captured in subtropical waters but are severely damaged upon collection (Nakamura and Suzuki 2015). We could not find any reference to the Medusettidae in contemporary studies off California and only a few worldwide (e.g., Cachon and Cachon-Enjume 1965). Only a handful of studies have reported the presence of large colonial Tuscaroridae (Ling and Haddock 1997) and Coelodendridae (Zasko and Rusanov 2005). For these taxa, in situ collection with remotely operated vehicles (Beittenmiller 2015), submersible vehicles (Swanberg et al. 1986) or in situ imaging (Nakamura et al. 2017) has enabled detailed observations. Regardless of differences in taxonomic resolution between this and previous studies, our detection of these elusive taxa at depth supports the increase in rhizarian diversity with depth near the CCE (Gulf of California; Zasko and Rusanov 2005) or elsewhere (e.g., highest phaeodarian diversity at ~ 7000 m in the Kamchatka, Reshetnyak 1955). This increase in diversity is inconsistent with the expected decrease in protistan diversity toward the mesopelagic (Robinson et al. 2010) but should be viewed as an example of adaptation of phaeodarians to deep-dwelling life. We have also confirmed the tendency for larger organisms to occur deeper in the water column, a typical feature not only of phaeodarians (Zasko and Rusanov 2005), but also numerous other deep-sea organisms (e.g., Bergmann's principle of increasing cell size with decreasing temperature; Timofeev 2001).

Vertical niche distribution and influence of environmental factors

In the upper layers of the CCE (0–200 m) most test-bearing rhizarians showed pronounced changes in abundances within and between cruises. Early on, it was reported that the upper 200 m off Southern California showed seasonal changes in rhizarian populations, depending on ocean circulation (Casey 1966). Notably, such seasonal fluctuations in rhizarian

assemblages were not reported deeper, in the mesopelagic layer (Casey 1971), a consistent pattern observed here. Further analyses should focus on resolving depth-dependent rhizarian population variability in the CCE with respect to ocean circulation and upwelling dynamics (e.g., Lavaniegos and Ohman 2007).

With images taken in situ every ~ 5–20 cm and binned to depths of 5 m, from the surface down to the mesopelagic layer, we were able to define the vertical niches of different taxa of test-bearing rhizarians at unprecedented resolution. Until the advent of in situ imaging techniques, vertical niche definition relied on the use of traditional sampling methods like plankton nets, Niskin bottles or pumps, all representing rather coarse vertical resolution, leading to broad estimates of vertical niches (Dworetzky and Morley 1987; Zasko and Rusanov 2005). Although four studies have used in situ imaging technologies for rhizarian habitat analyses (Dennett et al. 2002; Biard et al. 2016; Nakamura et al. 2017; Gaskell et al. 2019), none has analyzed fine-scale vertical distributions in relation to environmental variables. Nevertheless, our results overall are similar to previous assessments of the vertical ranges of polycystine radiolarians in the northern subtropical Pacific (Boltovskoy et al. 2017), although most of the organisms detected in the present study belong to the Phaeodaria (taxa not covered in Boltovskoy et al. 2017). Four major vertical zones were delineated by Boltovskoy et al. (2017): (1) species limited to surface waters (< 100 m), (2) species inhabiting the base of the euphotic zone (~ 100 m), (3) species from intermediate waters (100–300 m), and (4) deep-dwelling species (> 300 m). With only three vertical zones defined in the present study using in situ imagery, the earlier authors' vertical zonation is similar, the only difference being species inhabiting intermediate waters. We found two taxa, Medusettidae and Coelodendridae to be transitional between the base of epipelagic and upper mesopelagic zones, which would correspond to the earlier zonation.

We investigated the influence of environmental factors on rhizarians inhabiting these vertical layers at both aggregated and taxon-specific levels. The similarities we observed between both types of GAMs (i.e., aggregated taxa and taxon-specific) can be explained by the similarity of constraints acting on different taxa within a vertical stratum (e.g., groups harboring photosymbionts thriving in the illuminated epipelagic). The primary differences between types of GAMs related to overall model performance (i.e., R^2_{adj} , deviance explained, etc.). Such differences were likely a result of differences in numbers of data points, where GAMs including all taxa decrease the probability of null abundances. To further compare our results with existing knowledge on taxon-specific rhizarian ecology, we discuss GAMs by taxon below following the vertical zonation described previously.

Epipelagic zone

In the epipelagic layer (i.e., 0–100 m), both Collodaria and Acantharia were the dominant taxa, along with a few other

less common forms. The presence of both of these taxa in surface layers has been reported on several occasions and in contrasting ecosystems (e.g., Beers and Stewart 1971; Anderson 1983; Michaels 1988; Boltovskoy et al. 2017). This affinity with surface illuminated layers is likely related to the presence of photosymbionts in some acantharian cells (i.e., in three out of nine molecular clades; Decelle and Not 2015) and in almost all collodarian species (Hollande and Enjumet 1953). Notably, the non-symbiotic relatives of acantharians (Decelle and Not 2015) and collodarians (probably limited to the family Collophidiidae; Biard et al. 2017) have been observed deeper in the dark ocean (Schewiakoff 1926; Bernstein et al. 1999; Biard et al. 2017). Interestingly, although both have the ability to adjust their buoyancy and vertical position (Michaels 1988), physical mechanisms at the air–water interface (e.g., Langmuir cells or *zoöcurrent* as referred to by Haeckel 1893) can lead to increased concentration or patchiness in surface layers during periods of calm ocean conditions (Casey 1971; Swanberg 1983; Michaels 1988). Conversely, wind-driven disturbances could lead to decreased abundances of epipelagic rhizarians by mixing the community through the water column. This phenomenon could explain high acantharian densities observed in frontal regions in 2012 (Fig. 4b), a similar pattern observed in situ in a frontal zone of the Ligurian Current (Mediterranean Sea; Faillettaz et al. 2016).

In the surface layer, temperature significantly influenced collodarian and acantharian abundances, with lower abundances in waters cooler than 13–15°C. This pattern is consistent with previous studies, highlighting the importance of temperature (followed by nutrients and primary productivity) for radiolarian abundances and distribution in this layer (Dworetzky and Morley 1987; Boltovskoy and Correa 2016). While increases in collodarian abundances have been previously associated with increasing chlorophyll *a* concentration at the deep chlorophyll maximum (Faillettaz et al. 2016), here a deeper DCM also led to a decrease in abundances. Whether this is a cause-and-effect relationship is unclear, as chlorophyll *a* concentration at the DCM was negatively correlated with the depth of the DCM (Kendall's $T = -0.38$; $p < 0.001$, $n = 243$). Also, Chl *a* increases in deep water often reflect increased Chl *a* per cell rather than increased biomass. Yet, the limited statistical fits of overall GAM models suggest that variables other than temperature, chlorophyll *a* concentration or DCM, should be considered to fully understand abundance changes of epipelagic rhizarians. Given the mixotrophic nature of most epipelagic rhizarians, variability of food concentrations (e.g., bacteria, protists, etc.) and/or co-occurrence of free-living symbiont populations on epipelagic rhizarians should be evaluated, in addition to predators and parasites.

Lower epipelagic zone

At the base of the epipelagic zone, the CCE region was characterized by three phaeodarian groups: the abundant taxa Aulosphaeridae and Castanellidae, and less abundant Coelodendridae. Further south, in the Gulf of California, their

presence has been previously observed at similar depths, expected for the Aulosphaeridae, which were observed deeper and with considerably lower abundances (Zasko and Rusanov 2005). Elsewhere, these taxa have also been observed in slightly deeper layers (e.g., < 500 m in the South Atlantic; Kling and Boltovskoy 1995) where they can occupy a substantial fraction of zooplankton biomass (e.g., 2.7–13% at 200–300 m at station ALOHA; Steinberg et al. 2008). However, it has been hypothesized that the vertical distribution of test-bearing Rhizaria can vary with latitude, with some species found in shallow surface waters in high latitudes, but potentially in deeper layers in low latitudes (Casey 1977). This variability is believed to be related to water temperature, a factor constraining phaeodarian vertical distributions elsewhere (reviewed in Nakamura and Suzuki 2015). In a companion study to the present work, Aulosphaeridae were inversely correlated with the depth of the 10°C isotherm (Stukel et al. 2018). Here, in most cruises, the GAMs showed significant decreases of epipelagic phaeodarian populations with increasing temperature at the depth of their preferred habitat (~ 100 m). In addition to water temperature, food supply and dissolved silicon concentration are secondary limiting factors for phaeodarians (reviewed in Nakamura and Suzuki 2015).

Early on, it was hypothesized that deep-water rhizarians should be more abundant below regions of high productivity (Casey 1987). The GAMs generated for Aulosphaeridae and Castanellidae did not produce strong evidence to support increased phaeodarian abundances with enhanced particle concentrations (considered here as a proxy for the food of flux-feeders). Neither were relationships detected between the abundance of phaeodarians and the magnitude of carbon export, as determined using sediment traps or the ^{234}Th method. However, phaeodarians, known to be flux feeders (Gowing 1989), are also omnivores that feed on suspended bacteria and protists (Anderson 1983; Gowing 1986; Gowing and Wishner 1992). As little is known about phaeodarian ecology (Nakamura and Suzuki 2015), the relative importance of these two different diets is unknown. We cannot exclude the possibility that a lack of response to increased particle concentrations reflects a predominantly omnivorous diet in the lower epipelagic, and similar to epipelagic rhizarians (see above Section 3) the importance of biotic factors such as prey and predator availability is yet to be included in statistical models.

The GAMs for the two phaeodarian taxa inhabiting the lower epipelagic showed contrasting yet significant responses to increased dissolved silicon (dSi) concentrations, from slight decreases of Castanellidae abundances to moderate increases of Aulosphaeridae. For smaller phaeodarians, the availability of dSi could influence their vertical distribution, since some species migrate to layers of higher dSi concentrations (Okazaki et al. 2004). Here we did not find evidence of changes in vertical distribution over time, suggesting a rather stable positioning at ~ 100 m (see also Ohman et al. 2012), potentially corresponding to a habitat that optimizes phaeodarian

temperature preferences and food availability. In this scenario, dSi concentration would have a limited effect on lower epipelagic rhizarian communities, contrasting with observations from the upper mesopelagic.

Upper mesopelagic zone

Below the 200 m horizon in the CCE, in situ observations revealed a diverse rhizarian community, characterized mostly by large phaeodarians and planktonic foraminiferans, both with relatively stable abundances over time. Unlike their relatives from the lower epipelagic zone, the three testate phaeodarian taxa, Coelodendridae, Aulacanthidae and unknown phaeodarians, displayed a significant increase of abundance with increasing dSi in the mesopelagic layer. Together with the lack of or weak response to temperature and particle concentrations, this pattern is some of the first direct evidence that dSi availability may influence deep phaeodarian communities. Below a certain depth threshold, the decrease in water temperature (shown early on to be a major variable affecting phaeodarian vertical distribution; Nakamura et al. 2013) is slow and constant. Therefore, below a given temperature, phaeodarians are likely to meet favorable conditions to survive and grow at depth, but our results suggest that their success could then be partially constrained by dSi availability. However, as dSi concentrations are correlated with depth (and pressure), their effects could potentially be confounded with those of hydrostatic pressure. At this time, we still lack understanding of much fundamental rhizarian biology (Nakamura and Suzuki 2016; Suzuki and Not 2016), however, one early study suggested the lack of hydrostatic pressure effects on rhizarians, apparently due to the lack of gas-filled spaces in the cell (Funnell 1967). Although dSi concentrations turned out to be a significant predictor for all three mesopelagic phaeodarians, the overall GAM performances ($0.12 < R^2_{\text{adj}} < 0.26$) indicate that dSi plays only a minor role in the overall variations of phaeodarian abundances, and additional variables need to be considered. Nevertheless, we suggest that direct experimental work be undertaken to establish the concentrations of dSi over which Rhizaria saturate their rates of uptake.

In this layer, in situ observations also revealed that various test-bearing rhizarians thrive in oxygen depleted water (< 50 $\mu\text{mol kg}^{-1}$). Only digitate foraminifera (e.g., *Hastigerina* spp.), observed in the present study, have already been associated with the OMZ (Hull et al. 2011; Gaskell et al. 2019), while a similar pattern has not been clearly reported so far for phaeodarians. This association with the OMZ was believed to coincide with a peak in mesopelagic biomass, located above the OMZ, upon which the carnivorous digitate foraminifera depend for locating their prey (e.g., calanoid copepods; Hull et al. 2011). Given the omnivorous behavior of phaeodarians (Anderson 1983; Gowing 1986; Gowing and Wishner 1992), in situ observations of specimens covered with marine snow (Hull et al. 2011), and the lack of in situ images that could

support hypothesis of feeding by phaeodarians on metazoans, it seems likely that phaeodarians are less dependent on the OMZ position than their carnivorous relatives.

Beyond the role of abiotic factors on rhizarian populations

Although we modeled the effects of several environmental variables in three different vertical provinces, the moderate performances of most GAMs suggest that additional variables, other than those tested here, influence rhizarian abundances over time. For example, we cannot rule in or out the impact and importance of biotic interactions (i.e., predation, symbiosis, parasitism) in explaining distribution patterns and seasonal variations. However, in the current state, little is known about potential predators, parasites, or pathogens of test-bearing rhizarians. Early laboratory and field studies suggested that rhizarians are omnivores able to consume diverse types of prey ranging from bacteria (Gowing and Garrison 1992), protists (e.g., diatoms, tintinnids, dinoflagellates, etc.; Swanberg and Harbison 1979; Anderson et al. 1984; Gowing and Garrison 1992), to metazoans like copepods (Anderson 1978). The few predators reported so far include hyperiid amphipods (Swanberg and Harbison 1979) or lobster larvae (O'Rourke et al. 2012), while other taxa have been shown to avoid the consumption of rhizarians, potentially because of sterol compounds produced by photosymbiotic species (Swanberg 1979; Anderson 1983). To our knowledge, no comprehensive reports of test-bearing rhizarians have been made from the gut contents of mesopelagic metazoans. Therefore, although our GAM models explained a moderate percentage of deviance, our limited knowledge of biotic interactions with test-bearing rhizarians currently prevent the inclusion of biotic drivers in models.

Implications for rhizarian ecology and evolution

The present data provide insights into the evolution of test-bearing rhizarians with respect to their environment and competition with other silicifiers, diatoms in particular. Although radiolarians were among the first protistan lineages inhabiting the primitive ocean (Suzuki and Oba 2015), the decrease in dSi concentration during the Cenozoic (ca. 66 Ma), coupled with the rise of diatoms, led to a decrease in radiolarian silicification and ecological success (Lazarus et al. 2009). Here we distinguish three distinct vertical layers, which may reflect different biological adaptations. In surface layers of the CCE, where diatoms often dominate phytoplankton communities (e.g., Brzezinski et al. 2015; Taylor et al. 2015), two test-bearing rhizarians dominate in dSi poor water masses: (1) Collodaria, the most recent radiolarian lineage (ca. 40 Ma; Suzuki and Oba 2015), with two collodarian families (Sphaerorozoidae and Collophidiidae) out of three typically possessing simple silicified spines (e.g., *Sphaerorozoum*) or even lacking all silicified structures (Biard et al. 2015) and (2) Acantharia, which build tests of strontium sulfate. Both forms are therefore not influenced (or minimally influenced

for the few silicified collodarians) by the lack of dSi. Deeper, from the base of the euphotic zone to the deep and dark oceanic layers where diatoms are absent, dSi concentrations increase. Although the concentration of dSi to which phaeodarians respond remains unknown, large silicified phaeodarians become more diverse with depth and their abundance could be influenced by dSi availability as reflected by the present GAM results. Should the relationships between dissolved silicon and phaeodarian distribution prove to be physiologically relevant through experimental work, these results suggest the possible importance of dissolved silicon in structuring protistan communities from the surface to the deep mesopelagic ocean.

Conclusions

Interest in planktonic rhizarians has expanded markedly in the last two decades, thanks to the development of molecular techniques and in situ imaging (Caron 2016). Using non-invasive in situ imaging, here we found three primary vertical habitats of test-bearing planktonic Rhizaria in the upper 500 m of the water column off Southern California: epipelagic, lower epipelagic, and upper mesopelagic assemblages. A diverse community of Rhizaria thrives in the mesopelagic zone, where large silicified specimens are prevalent. Statistical modeling with Generalized Additive Models revealed that abundances of the dominant rhizarians in each of these zones are partially defined by: *Epipelagic*—temperature and Chl *a* at the DCM; *Lower epipelagic*—temperature and dissolved silicon concentrations; *Upper mesopelagic silicifiers*—silicic acid; *Upper mesopelagic Foraminifera*—dissolved oxygen. In order to better resolve and model abundance variability over time, future studies should treat the role of biotic interactions such as predation, symbiosis, and parasitism on different rhizarian taxa.

While the present study delineates the habitats of different categories of rhizarians, companion studies in this region evaluated biogeochemical impacts of selected taxa. Large phaeodarian Aulosphaeridae, together with Castanellidae, transport important amounts of biogenic silica to the deep ocean (Biard et al. 2018) and also play substantial roles in carbon flux attenuation in the mesopelagic (Stukel et al. 2018). Together, these studies suggest the need to represent larger planktonic Rhizaria in ecological and biogeochemical models, with explicit consideration of their depth-dependent impacts.

References

- Anderson, O. R. 1978. Light and electron microscopy observations of feeding behavior, nutrition, and reproduction in laboratory cultures of *Thalassicolla nucleata*. *Tissue Cell* **10**: 401–412. doi:[10.1016/S0040-8166\(16\)30336-6](https://doi.org/10.1016/S0040-8166(16)30336-6)
- Anderson, O. R. 1983. *Radiolaria*. Springer-Verlag.

- Anderson, O. R. 2012. Living together in the plankton: A survey of marine protist symbioses. *Acta Protozool.* **52**: 1–10. doi:[10.4467/16890027AP.13.006.1085](https://doi.org/10.4467/16890027AP.13.006.1085)
- Anderson, O. R., N. R. Swanberg, and P. Bennett. 1984. An estimate of predation rate and relative preference for algal versus crustacean prey by a spongioid skeletal radiolarian. *Mar. Biol.* **78**: 205–207. doi:[10.1007/BF00394702](https://doi.org/10.1007/BF00394702)
- Beers, J. R., and G. L. Stewart. 1970. The preservation of Acantharians in fixed plankton samples. *Limnol. Oceanogr.* **15**: 825–827. doi:[10.4319/lo.1970.15.5.0825](https://doi.org/10.4319/lo.1970.15.5.0825)
- Beers, J. R., and G. L. Stewart. 1971. Micro-zooplankters in the plankton communities of the upper waters of the eastern tropical Pacific. *Deep Sea Res. Oceanogr. Abstr.* **18**: 861–883. doi:[10.1016/0011-7471\(71\)90061-1](https://doi.org/10.1016/0011-7471(71)90061-1)
- Beittenmiller, K. 2015. Characterizing the geometry of Phaeodarian colonial spheres. Carnegie Mellon Univ..
- Benfield, M. C., P. Grosjean, and P. F. Culverhouse. et al 2007. RAPID: Research on automated plankton identification. *Oceanography* **20**: 172–187. doi:[10.5670/oceanog.2007.63](https://doi.org/10.5670/oceanog.2007.63)
- Bernstein, R. E., P. R. Betzer, R. A. Feely, R. H. Byrne, M. F. Lamb, and A. F. Michaels. 1987. Acantharian fluxes and strontium to chlorinity ratios in the North Pacific Ocean. *Science* **237**: 1490–1494. doi:[10.1126/science.237.4821.1490](https://doi.org/10.1126/science.237.4821.1490)
- Bernstein, R. E., S. A. Kling, and D. Boltovskoy. 1999. Acantharia, p. 77–147. In D. Boltovskoy [ed.], *South Atlantic Zooplankton*. Backhuys Publishers.
- Biard, T., L. Pillet, J. Decelle, C. Poirier, N. Suzuki, and F. Not. 2015. Towards an integrative morpho-molecular classification of the Collodaria (Polycystinea, Radiolaria). *Protist* **166**: 374–388. doi:[10.1016/j.protis.2015.05.002](https://doi.org/10.1016/j.protis.2015.05.002)
- Biard, T., L. Stemann, and M. Picheral. et al 2016. In situ imaging reveals the biomass of giant protists in the global ocean. *Nature* **532**: 504–507. doi:[10.1038/nature17652](https://doi.org/10.1038/nature17652)
- Biard, T., E. Bigeard, S. Audic, J. Poulain, A. Gutierrez-Rodriguez, S. Pesant, L. Stemann, and F. Not. 2017. Biogeography and diversity of Collodaria (Radiolaria) in the global ocean. *ISME J.* **11**: 1331–1344. doi:[10.1038/ismej.2017.12](https://doi.org/10.1038/ismej.2017.12)
- Biard, T., J. W. Krause, M. R. Stukel, and M. D. Ohman. 2018. The significance of giant Phaeodarians (Rhizaria) to biogenic silica export in the California current ecosystem. *Global Biogeochem. Cycles* **32**: 987–1004. doi:[10.1029/2018GB005877](https://doi.org/10.1029/2018GB005877)
- Boltovskoy, D., and W. R. Riedel. 1987. Polycystine radiolaria of the California current region: Seasonal and geographic patterns. *Mar. Micropaleontol.* **12**: 65–104. doi:[10.1016/0377-8398\(87\)90014-4](https://doi.org/10.1016/0377-8398(87)90014-4)
- Boltovskoy, D., and N. Correa. 2016. Biogeography of Radiolaria Polycystina (Protista) in the World Ocean. *Prog. Oceanogr.* **149**: 82–105. doi:[10.1016/j.pocean.2016.09.006](https://doi.org/10.1016/j.pocean.2016.09.006)
- Boltovskoy, D., O. R. Anderson, and N. M. Correa. 2017. Radiolaria and Phaeodaria, p. 731–763. In J. M. Archibald, A. G. B. Simpson, and C. H. Slamovits [eds.], *Handbook of the protists*. Springer International Publishing.
- Breheny, P., and W. Burchett. 2017. Visualization of regression models using visreg. *R J* **9**: 56–71. doi:[10.32614/RJ-2017-046](https://doi.org/10.32614/RJ-2017-046)
- Brzezinski, M. A., J. W. Krause, R. M. Bundy, K. A. Barbeau, P. Franks, R. Goericke, M. R. Landry, and M. R. Stukel. 2015. Enhanced silica ballasting from iron stress sustains carbon export in a frontal zone within the California current. *J. Geophys. Res. Oceans* **120**: 4654–4669. doi:[10.1002/2015JC010829](https://doi.org/10.1002/2015JC010829)
- Burki, F., and P. J. Keeling. 2014. Rhizaria. *Curr. Biol.* **24**: R103–R107. doi:[10.1016/j.cub.2013.12.025](https://doi.org/10.1016/j.cub.2013.12.025)
- Cachon, J., and M. Cachon-Enjumet. 1965. Étude cytologique et caryologique d'un Phaeodarié bathypélagique *Planktonetta atlantica* Borgert. *Bull. Inst. Océan. Monaco* **64**: 1–23.
- Caron, D. A. 2016. Ocean science: The rise of Rhizaria. *Nature* **532**: 444–445. doi:[10.1038/nature17892](https://doi.org/10.1038/nature17892)
- Caron, D. A., P. D. Countway, and M. V. Brown. 2004. The growing contributions of molecular biology and immunology to Protistan ecology: Molecular signatures as ecological tools. *J. Eukaryot. Microbiol.* **51**: 38–48. doi:[10.1111/j.1550-7408.2004.tb00159.x](https://doi.org/10.1111/j.1550-7408.2004.tb00159.x)
- Casey, R. E. 1971. Distribution of polycystine radiolaria in the oceans in relation to physical and chemical conditions, p. 151–159. In B. M. Funnell and W. R. Riedel [eds.], *The micropalaeontology of oceans*. Cambridge University Press.
- Casey, R. E. 1977. The ecology and distribution of recent radiolaria, p. 809–845. In A. T. S. Ramsey [ed.], *Oceanic micropalaeontology*. Academic Press.
- Casey, R. E. 1987. Radiolaria, p. 213–247. In T. W. Broadhead [ed.], *Fossil prokaryotes and protists*. University of Tennessee, Notes for a Short Course.
- Casey, R. E. 1966. A seasonal study on the distribution of polycystine radiolarians from waters overlying the Catalina basin, southern California. University of Southern California.
- Cowen, R. K., and C. M. Guigand. 2008. In situ ichthyoplankton imaging system (ISIS): System design and preliminary results. *Limnol. Oceanogr. Methods* **6**: 126–132. doi:[10.4319/lom.2008.6.126](https://doi.org/10.4319/lom.2008.6.126)
- Davis, C. S., S. Gallager, M. Berman, L. Haury, and J. Strickler. 1992a. The – (VPR): Design and initial results. *Arch. Hydrobiol. Beih.* **36**: 67–81.
- Davis, C. S., S. M. Gallager, and A. R. Solow. 1992b. Microaggregations of oceanic plankton observed by towed video microscopy. *Science* **257**: 230–232. doi:[10.1126/science.257.5067.230](https://doi.org/10.1126/science.257.5067.230)
- Decelle, J., S. Colin, and R. A. Foster. 2015. Photosymbiosis in marine planktonic protists, p. 465–500. In S. Ohtsuka, T. Suzuki, T. Horiguchi, N. Suzuki, and F. Not [eds.], *Marine protists*. Japan: Springer.
- Decelle, J., and F. Not. 2015. Acantharia, p. 1–10. In eLS. John Wiley & Sons Ltd.
- Dennett, M. R., D. A. Caron, A. F. Michaels, S. M. Gallager, and C. S. Davis. 2002. Video plankton recorder reveals high

- abundances of colonial Radiolaria in surface waters of the central North Pacific. *J. Plankton Res.* **24**: 797–805. doi:[10.1093/plankt/24.8.797](https://doi.org/10.1093/plankt/24.8.797)
- Dworetzky, B. A., and J. J. Morley. 1987. Vertical distribution of radiolaria in the eastern equatorial Atlantic: Analysis of a multiple series of closely-spaced plankton tows. *Mar. Micro-paleontol.* **12**: 1–19. doi:[10.1016/0377-8398\(87\)90011-9](https://doi.org/10.1016/0377-8398(87)90011-9)
- Erez, J. 2003. The source of ions for biomineralization in foraminifera and their implications for paleoceanographic proxies. *Rev. Mineral. Geochem.* **54**: 115–149. doi:[10.2113/0540115](https://doi.org/10.2113/0540115)
- Faillietaz, R., M. Picheral, J. Y. Luo, C. Guigand, R. K. Cowen, and J.-O. Irisson. 2016. Imperfect automatic image classification successfully describes plankton distribution patterns. *Methods Oceanogr.* **15–16**: 60–77. doi:[10.1016/j.mio.2016.04.003](https://doi.org/10.1016/j.mio.2016.04.003)
- Funnell, B. M. 1967. Foraminifera and Radiolaria as depth indicators in the marine environment. *Mar. Geol.* **5**: 333–347. doi:[10.1016/0025-3227\(67\)90044-8](https://doi.org/10.1016/0025-3227(67)90044-8)
- Gaskell, D. E., M. D. Ohman, and P. M. Hull. 2019. Zooglider-based measurements of planktonic foraminifera in the California current system. *J. Foram. Res.* **49**: 390–404. doi:[10.2113/gsjfr.49.4.390](https://doi.org/10.2113/gsjfr.49.4.390)
- Gowing, M. M. 1986. Trophic biology of phaeodarian radiolarians and flux of living radiolarians in the upper 2000 m of the North Pacific central gyre. *Deep Sea Res. Part Oceanogr. Res. Pap.* **33**: 655–674. doi:[10.1016/0198-0149\(86\)90059-2](https://doi.org/10.1016/0198-0149(86)90059-2)
- Gowing, M. M. 1989. Abundance and feeding ecology of Antarctic phaeodarian radiolarians. *Mar. Biol.* **103**: 107–118. doi:[10.1007/BF00391069](https://doi.org/10.1007/BF00391069)
- Gowing, M. M., and D. L. Garrison. 1992. Abundance and feeding ecology of larger protozooplankton in the ice edge zone of the Weddell and Scotia Seas during the austral winter. *Deep Sea Res. Part Oceanogr. Res. Pap.* **39**: 893–919. doi:[10.1016/0198-0149\(92\)90128-G](https://doi.org/10.1016/0198-0149(92)90128-G)
- Gowing, M. M., and K. F. Wishner. 1992. Feeding ecology of benthopelagic zooplankton on an eastern tropical Pacific seamount. *Mar. Biol.* **112**: 451–467. doi:[10.1007/BF00356291](https://doi.org/10.1007/BF00356291)
- Greer, A. T., R. K. Cowen, C. M. Guigand, and J. A. Hare. 2015. Fine-scale planktonic habitat partitioning at a shelf-slope front revealed by a high-resolution imaging system. *J. Mar. Syst.* **142**: 111–125. doi:[10.1016/j.jmarsys.2014.10.008](https://doi.org/10.1016/j.jmarsys.2014.10.008)
- Guidi, L., S. Chaffron, and L. Bittner. et al 2016. Plankton networks driving carbon export in the oligotrophic ocean. *Nature* **532**: 465–470. doi:[10.1038/nature16942](https://doi.org/10.1038/nature16942)
- Guisan, A., T. C. Edwards, and T. Hastie. 2002. Generalized linear and generalized additive models in studies of species distributions: Setting the scene. *Ecol. Model.* **157**: 89–100. doi:[10.1016/S0304-3800\(02\)00204-1](https://doi.org/10.1016/S0304-3800(02)00204-1)
- Haeckel, E. H. P. A. 1893. Planktonic studies: A comparative investigation of the importance and constitution of the pelagic fauna and flora. Rep. Comm. 1889-1891 U. S. Comm. Fish Fish., v. **17**. p. 565–641, Washington, Government printing office.
- Haecker, V. 1908. Tiefsee-Radiolarien. Spezieller Teil. Tripyleen, Collodarien und Mikroradiolarien der Tiefsee. *Wiss. Ergeb. Dtsch. Tiefsee-Exped. 'Valdivia' 1898–1899* **14**: 1–476.
- Hastie, T., and R. Tibshirani. 1986. Generalized additive models. *Stat. Sci.* **1**: 297–318. doi:[10.1214/ss/1177013604](https://doi.org/10.1214/ss/1177013604)
- Hollande, A., and M. Enjume. 1953. Contribution à l'étude biologique des Sphaerocollides (Radiolaires Collodaires et Radiolaires polycytaires) et de leurs parasites. *Ann. Sci. Nat. Zool.* **15**: 99–183.
- Hull, P. M., K. J. Osborn, R. D. Norris, and B. H. Robison. 2011. Seasonality and depth distribution of a mesopelagic foraminifer, *Hastigerinella digitata*, in Monterey Bay, California. *Limnol. Oceanogr.* **56**: 562–576. doi:[10.4319/lo.2011.56.2.0562](https://doi.org/10.4319/lo.2011.56.2.0562)
- Kendall, M., and J. D. Gibbons. 1990. Rank correlation methods, 5th ed. Oxford Univ. Press.
- Kimoto, K. 2015. Planktic foraminifera, p. 129–178. *In* S. Ohtsuka, T. Suzuki, T. Horiguchi, N. Suzuki, and F. Not [eds.], *Marine protists*. Japan: Springer.
- Kling, S. A., and D. Boltovskoy. 1995. Radiolarian vertical distribution patterns across the Southern California current. *Deep Sea Res. Part Oceanogr. Res. Pap.* **42**: 191–231. doi:[10.1016/0967-0637\(94\)00038-T](https://doi.org/10.1016/0967-0637(94)00038-T)
- Lampitt, R. S., I. Salter, and D. Johns. 2009. Radiolaria: Major exporters of organic carbon to the deep ocean. *Global Biogeochem. Cycles* **23**: GB1010. doi:[10.1029/2008GB003221](https://doi.org/10.1029/2008GB003221)
- Landry, M. R., M. D. Ohman, R. Goericke, M. R. Stukel, and K. Tsyklevich. 2009. Lagrangian studies of phytoplankton growth and grazing relationships in a coastal upwelling ecosystem off Southern California. *Prog. Oceanogr.* **83**: 208–216. doi:[10.1016/j.pocean.2009.07.026](https://doi.org/10.1016/j.pocean.2009.07.026)
- Lavaniegos, B. E., and M. D. Ohman. 2007. Coherence of long-term variations of zooplankton in two sectors of the California current system. *Prog. Oceanogr.* **75**: 42–69. doi:[10.1016/j.pocean.2007.07.002](https://doi.org/10.1016/j.pocean.2007.07.002)
- Lazarus, D., B. Kotrc, G. Wulf, and D. Schmidt. 2009. Radiolarians decreased silicification as an evolutionary response to reduced Cenozoic Ocean silica availability. *Proc. Natl. Acad. Sci. U. S. A.* **106**: 9333–9338. doi:[10.1073/pnas.0812979106](https://doi.org/10.1073/pnas.0812979106)
- Ling, H.-Y., and S. H. D. Haddock. 1997. The enclosing latticed sphere of *Tuscaridium cygneum* (Murray), a eurybathyal phaeodarian Radiolaria, from the North Pacific. *Paleontol. Res.* **1**: 144–149. doi:[10.2517/prpsj.1.144](https://doi.org/10.2517/prpsj.1.144)
- Luo, J. Y., B. Grassian, D. Tang, J. Irisson, A. T. Greer, C. M. Guigand, S. McClatchie, and R. K. Cowen. 2014. Environmental drivers of the fine-scale distribution of a gelatinous zooplankton community across a mesoscale front. *Mar. Ecol. Prog. Ser.* **510**: 129–149. doi:[10.3354/meps10908](https://doi.org/10.3354/meps10908)
- Massana, R. 2015. Protistan diversity in environmental molecular surveys, p. 3–21. *In* S. Ohtsuka, T. Suzuki, T. Horiguchi,

- N. Suzuki, and F. Not [eds.], Marine protists: Diversity and dynamics. Japan: Springer.
- Michaels, A. F. 1988. Vertical distribution and abundance of Acantharia and their symbionts. *Mar. Biol.* **97**: 559–569. doi:[10.1007/BF00391052](https://doi.org/10.1007/BF00391052)
- Nakamura, Y., I. Imai, A. Yamaguchi, A. Tuji, and N. Suzuki. 2013. *Aulographis japonica* sp. nov. (Phaeodaria, Aulacanthida, Aulacanthidae), an abundant zooplankton in the deep sea of the sea of Japan. *Plankton Benthos Res.* **8**: 107–115. doi:[10.3800/pbr.8.107](https://doi.org/10.3800/pbr.8.107)
- Nakamura, Y., and N. Suzuki. 2015. Phaeodaria: Diverse marine Cercozoans of world-wide distribution, p. 223–249. *In* S. Ohtsuka, T. Suzaki, T. Horiguchi, N. Suzuki, and F. Not [eds.], Marine protists. Japan: Springer.
- Nakamura, Y., R. Somiya, N. Suzuki, M. Hidaka-Umetsu, A. Yamaguchi, and D. J. Lindsay. 2017. Optics-based surveys of large unicellular zooplankton: A case study on radiolarians and phaeodarians. *Plankton Benthos Res.* **12**: 95–103. doi:[10.3800/pbr.12.95](https://doi.org/10.3800/pbr.12.95)
- Ohman, M. D. 2018. Introduction to collection of papers on the response of the southern California current ecosystem to the warm anomaly and El Niño, 2014–16. *Deep Sea Res. Part Oceanogr. Res. Pap.* **140**: 1–3. doi:[10.1016/j.dsr.2018.08.011](https://doi.org/10.1016/j.dsr.2018.08.011)
- Ohman, M. D. 2019. A sea of tentacles: Optically discernible traits resolved from planktonic organisms *in situ*. *ICES J. Mar. Sci.* **76**: 1959–1972. doi:[10.1093/icesjms/fsz184](https://doi.org/10.1093/icesjms/fsz184)
- Ohman, M. D., J. R. Powell, M. Picheral, and D. W. Jensen. 2012. Mesozooplankton and particulate matter responses to a deep-water frontal system in the southern California current system. *J. Plankton Res.* **34**: 815–827. doi:[10.1093/plankt/fbs028](https://doi.org/10.1093/plankt/fbs028)
- Ohman, M. D., K. Barbeau, P. Franks, R. Goericke, M. Landry, and A. Miller. 2013. Ecological transitions in a coastal upwelling ecosystem. *Oceanography* **26**: 210–219. doi:[10.5670/oceanog.2013.65](https://doi.org/10.5670/oceanog.2013.65)
- Ohman, M. D., R. E. Davis, J. T. Sherman, K. R. Grindley, B. M. Whitmore, C. F. Nickels, and J. S. Ellen. 2018. Zoolglider: An autonomous vehicle for optical and acoustic sensing of zooplankton. *Limnol. Oceanogr. Methods.* **17**: 69–86. doi:[10.1002/lom3.10301](https://doi.org/10.1002/lom3.10301)
- Okazaki, Y., K. Takahashi, T. Itaki, and Y. Kawasaki. 2004. Comparison of radiolarian vertical distributions in the Okhotsk Sea near the Kuril Islands and in the northwestern North Pacific off Hokkaido Island. *Mar. Micropaleontol.* **51**: 257–284. doi:[10.1016/j.marmicro.2004.01.003](https://doi.org/10.1016/j.marmicro.2004.01.003)
- O'Rourke, R., S. Lavery, and S. Chow. and others 2012. Determining the diet of larvae of Western rock lobster (*Panulirus cygnus*) using high-throughput DNA sequencing techniques. *PLoS One* **7**: e42757. doi:[10.1371/journal.pone.0042757](https://doi.org/10.1371/journal.pone.0042757)
- Picheral, M. 2017. EcoTaxa, a tool for the taxonomic classification of images. <http://ecotaxa.obs-vlfr.fr>.
- Picheral, M., L. Guidi, L. Stemmann, D. M. Karl, G. Iddaoud, and G. Gorsky. 2010. The underwater vision profiler 5: An advanced instrument for high spatial resolution studies of particle size spectra and zooplankton. *Limnol. Oceanogr. Methods* **8**: 462–473. doi:[10.4319/lom.2010.8.462](https://doi.org/10.4319/lom.2010.8.462)
- Remsen, A., T. L. Hopkins, and S. Samson. 2004. What you see is not what you catch: A comparison of concurrently collected net, optical plankton counter, and shadowed image particle profiling evaluation recorder data from the North-east Gulf of Mexico. *Deep Sea Res. Part Oceanogr. Res. Pap.* **51**: 129–151. doi:[10.1016/j.dsr.2003.09.008](https://doi.org/10.1016/j.dsr.2003.09.008)
- Reshetnyak, V. 1955. Vertical distribution of radiolarians in the Kuril-Kamchatka trench. *Tr. Zool. Inta Akad. Nauk SSSR* **21**: 94–101.
- Robinson, C., D. K. Steinberg, and T. R. Anderson. et al 2010. Mesopelagic zone ecology and biogeochemistry – A synthesis. *Deep Sea Res. Part II Top. Stud. Oceanogr.* **57**: 1504–1518. doi:[10.1016/j.dsr2.2010.02.018](https://doi.org/10.1016/j.dsr2.2010.02.018)
- Schewiakoff, W. T. 1926. The Acantharia, p. 1–755. *In* Fauna E Flora Golfo Napoli, v. **37**: 1–755.
- Simpson, A. G. B., C. H. Slamovits, and J. M. Archibald. 2017. Protist diversity and eukaryote phylogeny, p. 1–21. *In* J. M. Archibald, A. G. B. Simpson, and C. H. Slamovits [eds.], Handbook of the protists. Springer International Publishing.
- Steinberg, D. K., J. S. Cope, S. E. Wilson, and T. Kobari. 2008. A comparison of mesopelagic mesozooplankton community structure in the subtropical and subarctic North Pacific Ocean. *Deep Sea Res. Part II Top. Stud. Oceanogr.* **55**: 1615–1635. doi:[10.1016/j.dsr2.2008.04.025](https://doi.org/10.1016/j.dsr2.2008.04.025)
- Stukel, M. R., T. Biard, J. Krause, and M. D. Ohman. 2018. Large Phaeodaria in the twilight zone: Their role in the carbon cycle. *Limnol. Oceanogr.* **63**: 2579–2594. doi:[10.1002/lno.10961](https://doi.org/10.1002/lno.10961)
- Suzuki, N., and F. Not. 2015. Biology and ecology of Radiolaria, p. 179–222. *In* S. Ohtsuka, T. Suzaki, T. Horiguchi, N. Suzuki, and F. Not [eds.], Marine Protists. Japan: Springer.
- Suzuki, N., and M. Oba. 2015. Oldest fossil records of marine protists and the geologic history toward the establishment of the modern-type marine protist world, p. 359–394. *In* S. Ohtsuka, T. Suzaki, T. Horiguchi, N. Suzuki, and F. Not [eds.], Marine protists. Japan: Springer.
- Swanberg, N. R. 1979. The ecology of colonial radiolarians: their colony morphology, trophic interactions and associations, behavior, distribution, and the photosynthesis of their symbionts. Massachusetts Institute of Technology and Woods Hole Oceanographic Institution.
- Swanberg, N. R. 1983. The trophic role of colonial Radiolaria in oligotrophic oceanic environments. *Limnol. Oceanogr.* **28**: 655–666. doi:[10.4319/lo.1983.28.4.0655](https://doi.org/10.4319/lo.1983.28.4.0655)
- Swanberg, N. R., and G. R. Harbison. 1979. The ecology of Collozoum longiforme, sp. nov., a new colonial radiolarian from the equatorial Atlantic Ocean. *Deep Sea Res. Part Oceanogr. Res. Pap.* **27**: 715–732. [https://doi.org/10.1016/0198-0149\(80\)90024-2](https://doi.org/10.1016/0198-0149(80)90024-2)

- Swanberg, N., P. Bennett, J. L. Lindsey, and O. R. Anderson. 1986. The biology of a coelodendrid: A mesopelagic phaeodarian radiolarian. *Deep Sea Res. Part Oceanogr. Res. Pap.* **33**: 15–25. doi:[10.1016/0198-0149\(86\)90105-6](https://doi.org/10.1016/0198-0149(86)90105-6)
- Taylor, F. J. R. 1982. Symbioses in marine microplankton. *Ann. Inst. Océan.* **58**: 61–90.
- Taylor, A. G., M. R. Landry, K. E. Selph, and J. J. Wokuluk. 2015. Temporal and spatial patterns of microbial community biomass and composition in the southern California current ecosystem. *Deep Sea Res. Part II* **112**: 117–128. doi:[10.1016/j.dsr2.2014.02.006](https://doi.org/10.1016/j.dsr2.2014.02.006)
- Timofeev, S. F. 2001. Bergmann's principle and deep-water gigantism in marine crustaceans. *Biol. Bull. Russ. Acad. Sci.* **28**: 646–650. doi:[10.1023/A:1012336823275](https://doi.org/10.1023/A:1012336823275)
- Wickham, H., and RStudio. 2017. tidyverse: Easily install and load “Tidyverse” packages.
- Wiebe, P. H., and M. C. Benfield. 2003. From the Hensen net toward four-dimensional biological oceanography. *Prog. Oceanogr.* **56**: 7–136. doi:[10.1016/S0079-6611\(02\)00140-4](https://doi.org/10.1016/S0079-6611(02)00140-4)
- Wood, S. N. 2017. Generalized additive models: An introduction with R, 2nd ed. Chapman and Hall/CRC.
- Worden, A. Z., M. J. Follows, S. J. Giovannoni, S. Wilken, A. E. Zimmerman, and P. J. Keeling. 2015. Rethinking the marine carbon cycle: Factoring in the multifarious lifestyles of microbes. *Science* **347**: 1257594. doi:[10.1126/science.1257594](https://doi.org/10.1126/science.1257594)
- Zaba, K. D., and D. L. Rudnick. 2016. The 2014–2015 warming anomaly in the Southern California current system observed by underwater glider. *Geophys. Res. Lett.* **43**: 1241–1248. doi:[10.1002/2015GL067550](https://doi.org/10.1002/2015GL067550)
- Zasko, D. N., and I. I. Rusanov. 2005. Vertical distribution of radiolarians and their role in epipelagic communities of the East Pacific rise and the Gulf of California. *Biol. Bull.* **32**: 279–287. doi:[10.1007/s10525-005-0103-5](https://doi.org/10.1007/s10525-005-0103-5)

Acknowledgments

We thank Y. Nakamura and N. Suzuki for their help with the taxonomic outline of Rhizaria. We thank Linda Lanniello, Dr. Katsunori Kimoto, and Dr. Shinji Shimode for sharing some of their remarkable plankton images, and Sven Gastauer for advice with GAMs. We are grateful to M. Picheral for his help handling the UVP5 data and the operators who conducted UVP5 deployments during CCE-LTER process cruises. This work was supported by the Scripps Postdoctoral Fellowship award to TB, National Science Foundation grants OCE-1637632 and OCE-1614359 that support the CCE-LTER site, and a Gordon and Betty Moore Foundation award to MDO. This study is also a contribution from the CHAIRE Vision, supported by the CNRS and Sorbonne University and the French Investissements d’Avenir program.

Conflict of Interest

None declared.

Submitted 09 September 2019

Revised 16 April 2020

Accepted 26 April 2020

Associate editor: Susanne Menden-Deuer

Supplementary Text for:

Vertical niche definition of test-bearing protists (Rhizaria) into the twilight zone revealed by in situ imaging

Tristan Biard^{1,2}, Mark D. Ohman²

¹ Univ. Littoral Côte d'Opale, Univ. Lille, CNRS, UMR 8187, LOG, Laboratoire d'Océanologie et de Géosciences, F 62930 Wimereux, France.

² Scripps Institution of Oceanography, University of California, San Diego, La Jolla, CA 92093, USA

*Corresponding Author: tristan.biard@univ-littoral.fr

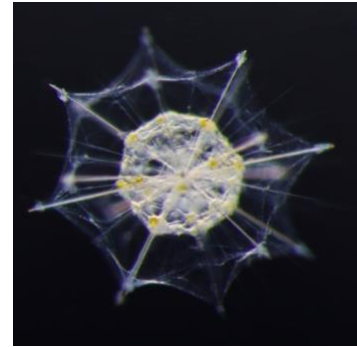
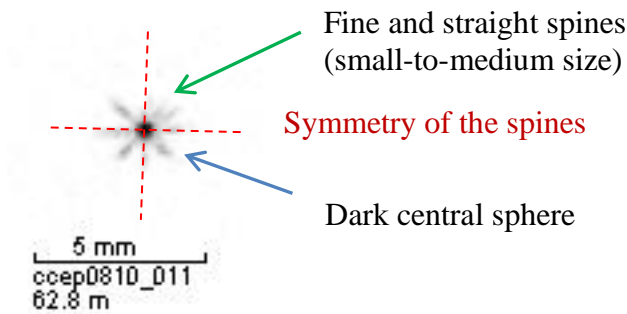
Appendix 1 – Taxonomic guide to rhizarian identification based on UVP5 images

Classification of the rhizarian categories with respect to higher taxonomic ranks (after: Adl et al. 2019; Nakamura and Suzuki 2015).

Phylum	Sub-phylum	Class	Order	Category	Fig1
Rhizaria	Retaria	Polycystinea	Collodaria	Collodaria	1a
		Acantharea	-	Acantharia	1b
		Foraminifera	-	Foraminifera	1g
	Cerczoa	Thecofilosea	Phaeodarea	Aulacanthida	1h
				Aulosphaeridae	1d
				Cannosphaeridae	1j
				Castanellidae	1c
				Tuscaroridae	1l
				Phaeogromida	1f
				Phaeodendrida	1i
				Phaeodaria (Circoporidae?)	1k
				-	-
				Rhizaria (unknown)	1e
	-	-	-	-	-

Below, we describe each category individually with the key morphological features used for identification. Each category is discussed using the same vignettes shown in Figures 1 and 2.

1. Acantharia



© Dr. Shinji Shimode

Identification: With their typical star-like shapes, acantharians cells are easily identified by the presence of **symmetry between two opposed spines**. The number of these spines varies between specimens and is not informative.

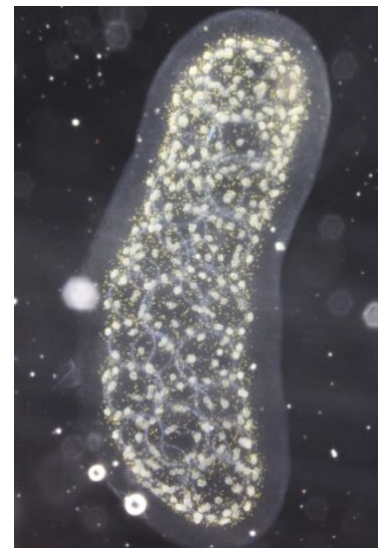
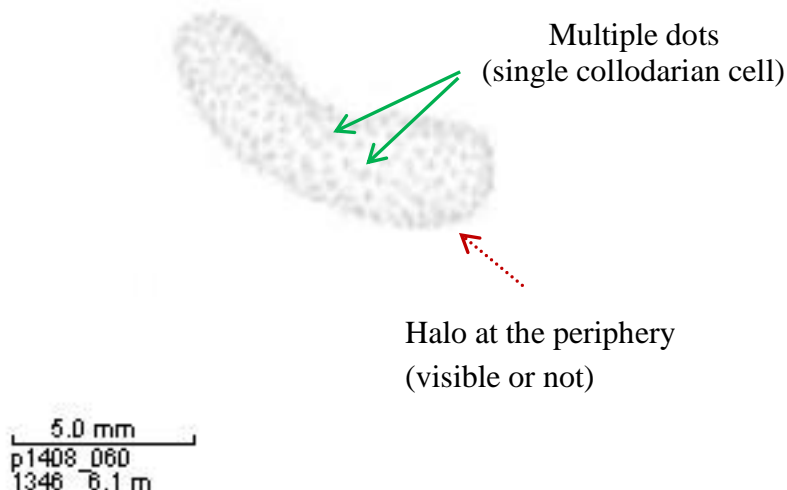
Supplementary criteria: As several acantharians species host photosymbionts, acantharians are more likely to be found in the euphotic zone.

Confusion with other categories: The symmetry of the cell is often the most informative criterion and cannot be confused with other categories where projections are not symmetrical. Could be confused with **Foraminifera**, **Coelodendridae** or **Phaeodaria (Circoporidae?)**.

2. Collodaria

Collodarians display two main shape: colonial form and solitary forms.

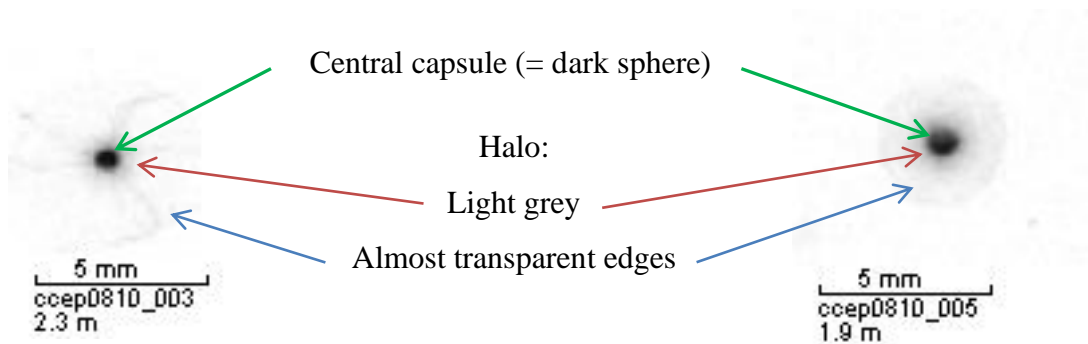
Oblong colonial collodarian



Identification: Colonial collodarians are easily identified because of their large size, the presence of **multiple cells** embedded within a same specimen, and often the presence of a **halo surrounding the colony**.

Confusion with other categories: no confusion likely.

Solitary collodarians

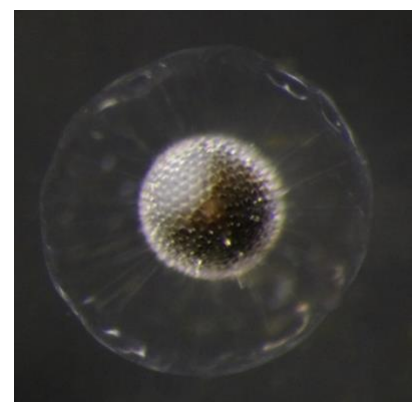
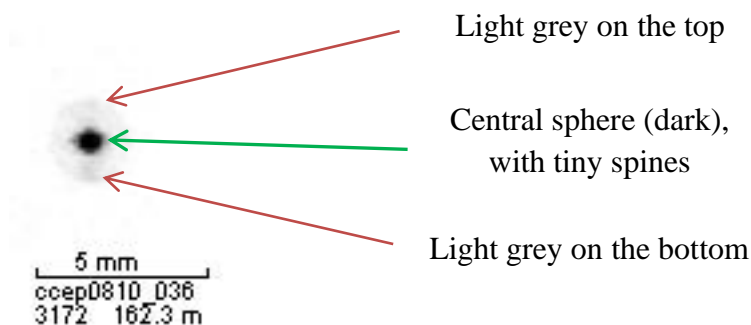


Identification: Unlike their colonial relatives, solitary collodarians are composed of one unique single cell with a large size. The solitary collodarian is composed of one **central capsule (dark)** in its center and often a large halo surrounding the central capsule. This halo is characterized by a **gradient of grey** from the inner part (light grey) to the **outer edges (white or almost transparent)**. Often, arm-like projections (grey) can be seen inside the halo (see image on the left-hand side).

Confusion with other categories: The main confusion comes from the **Castanellidae** that display the same spherical shape with halo. However, the gradient of grey is crucial to discriminate both categories. The gradient is absent in Castanellidae. **Aulosphaeridae** have the same spherical shape, but the edges of the sphere are clearly defined by a darker grey limit. **Cannosphaeridae** can be easily distinguished from solitary collodarians based on the alveolated pattern in the halo.

Supplementary criteria: Like acantharians, all known collodarian species described so far host photosymbionts. Therefore, they are more likely to be found in the euphotic zone.

3. Castanellidae



© Dr. Katsunori Kimoto

Identification: Castanellidae are composed of one unique single cell with a medium size. The specimen is composed of one **dark central sphere** (malacoma + scleracoma) with small spines visible at the periphery. The entire central sphere is surrounded by an extended network of ectoplasm (grey sphere) with **two darker areas visible at the top and the bottom** of the specimen. The thickness of the ectoplasm is equivalent to the diameter of the central sphere.

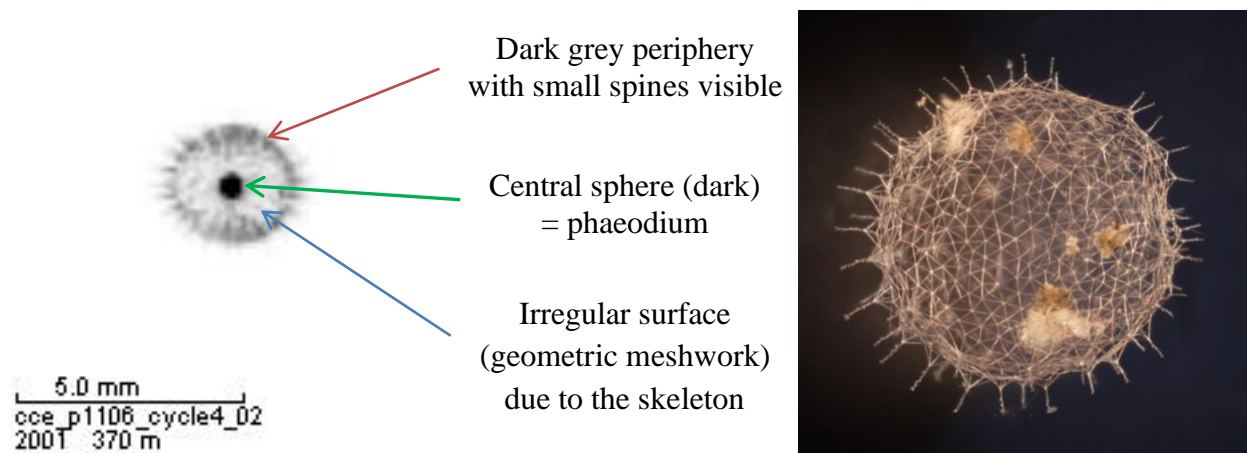
Confusion with other categories: confusion with **solitary collodarians** as described previously.

Supplementary criteria: None.

Remarks: **Castanellidae** can be found as colonies of several individual specimens, as shown in Figure 1.c (images with depths = 322 and 250 m).

4. Aulosphaeridae

Aulosphaeridae display two main shape: spherical and ovoid.

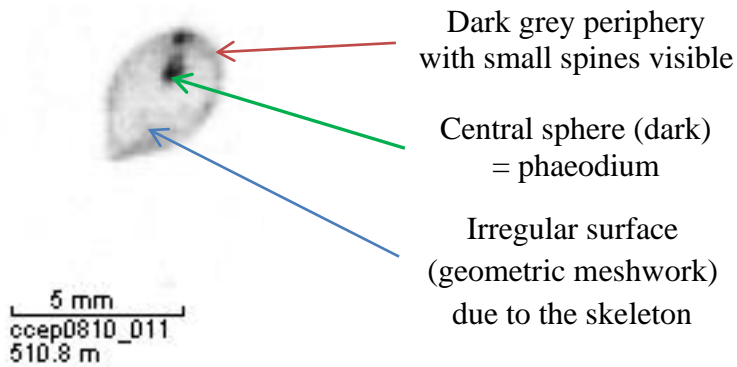


Identification: Aulosphaeridae are observed as sphere of medium size with a **geometric meshwork** (skeleton) at the surface, with **numerous short spines** often visible at the periphery, and, in its center, a clearly visible **phaeodium**.

Confusion with other categories: Possible confusion with **solitary collodarians** as described previously.

Supplementary criteria: None.

Remarks: **Aulosphaeridae** can be found as pairs or colonies of several individual specimens, as shown in Figure 1.c (images with depths = 91, 308, or 782 m).



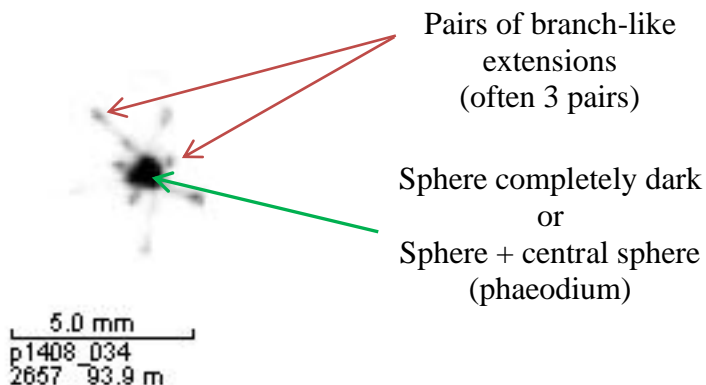
Identification: ‘Ovoid’ **Aulosphaeridae** appear similar to the spherical morphology, but the overall shape is an elongated sphere (= ovoid-like). The position of the central dark part is variable.

Putative taxonomic affiliation \equiv *Aulatractus* spp.

5. Rhizaria unknown

Identification: This category includes images that share some similar morphologies as the others described here but fail to meet all criteria required to be identified as one of these categories. Sphericity and the presence of a dark central sphere are two elements that distinguish these images from taxa other than rhizarians.

6. Medusettidae



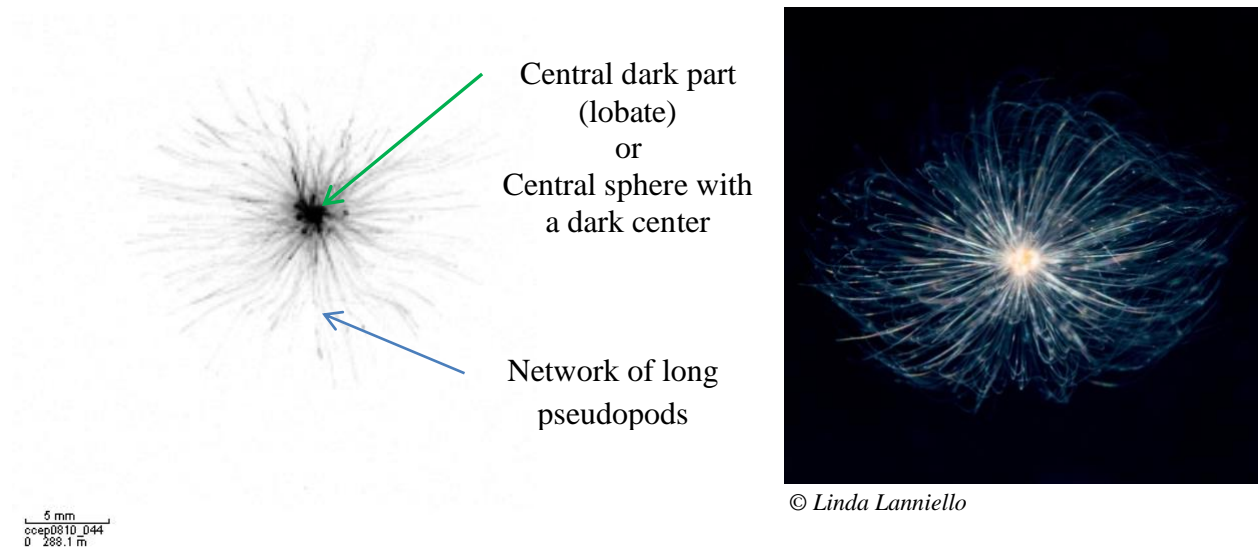
Identification: **Medusettidae** have an **ovoid central part** (completely black or with a phaeodium visible in its center), from which (often) three **pairs of long branch-like extensions** (styles) arise and projected outward.

Confusion with other categories: Possible confusion with **Coelodendridae**, but the latter lacking these pairs of styles (= styles organized individually).

Supplementary criteria: None.

Remarks: **Medusettidae** can be found as pairs or colonies of several individual specimens, as shown in Figure 1.f (image with depth = 365 m).

7. Foraminifera



Identification: Foraminifera observed in situ display a typical morphology consisting of a **central dark part (quasi-spherical or lobate chambers)** from which multiple **long pseudopods** arise and form a dense network, reaching up to ten times the size of the central test.

Confusion with other categories: Possible confusion with **acantharians** as described previously; with some **Aulacanthidae**, but the former having longer pseudopods with often hair-like structures; with some **Coelodendridae** having long styles but limited to 4-6 per specimen, unlike the dozens of pseudopods found in foraminiferans.

Supplementary criteria: None.

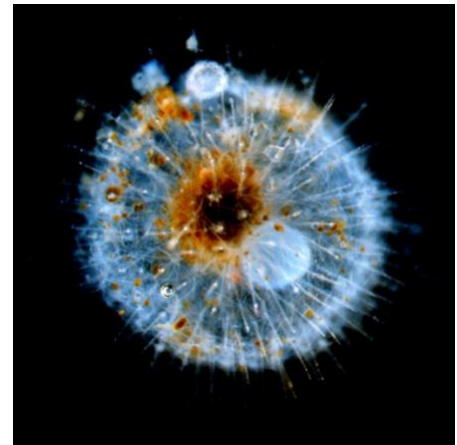
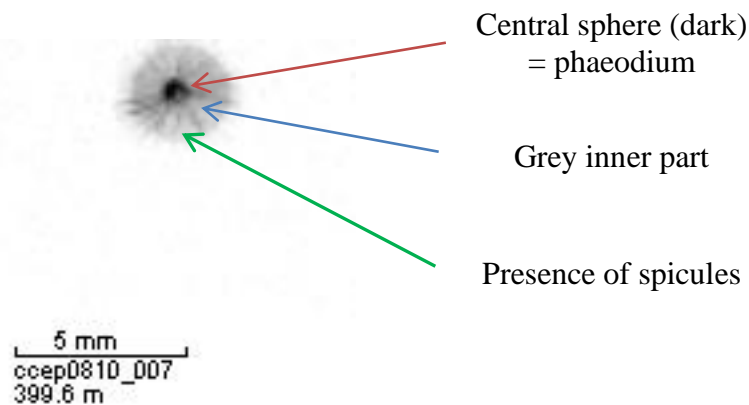
Remarks: None.

8. Aulacanthidae

Aulacanthidae observed in situ can be separated into three main morphotypes (not necessarily linked to specific taxa):

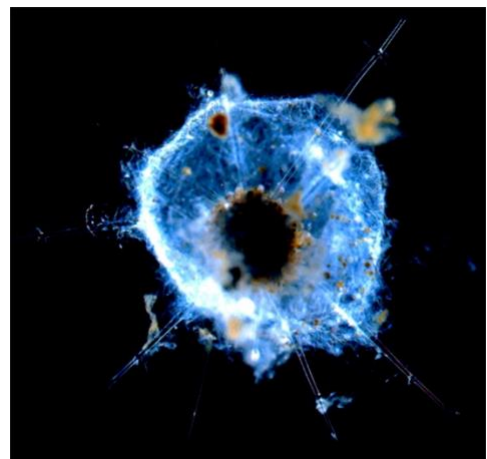
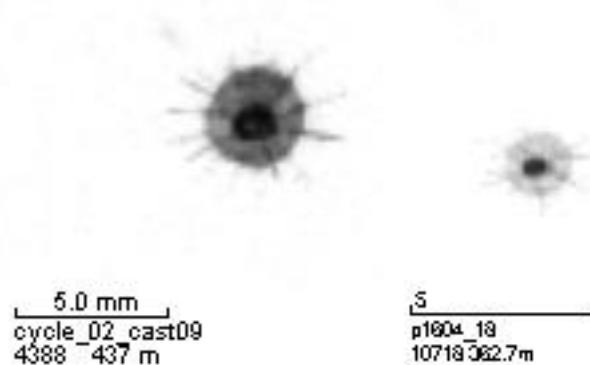
- Aulacanthidae ‘simple sphere’
- Aulacanthidae ‘spiky’
- Aulacanthidae ‘star’

Aulacanthidae ‘simple sphere’



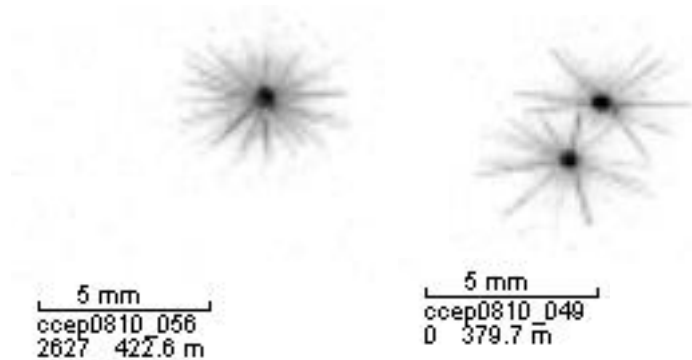
Identification: Aulacanthidae ‘simple sphere’ is a spherical organism with a **dark central phaeodium** in its center. The phaeodium is surrounded by a **homogeneous dark sphere** and from the phaeodium arise several **spicules** going beyond the periphery of the **main sphere**.

Aulacanthidae ‘spiky’



Identification: Aulacanthidae ‘spiky’ share the same general features as the previous Aulacanthidae category. However, these ‘spiky’ forms possess larger spicules, almost twice the size of the ‘simple sphere’

Aulacanthidae ‘star’



Identification: Aulacanthidae ‘star’ also share the same general features as the previous Aulacanthidae categories. However, these ‘star’ forms possess larger spicules, almost twice the size of the ‘simple sphere’, and more numerous spicules compared to the ‘spiky’ form.

Confusion with other categories: Possible confusion with **Acantharia**, but spicules shown here are not symmetrical; possible confusion with **Foraminifera**, but the latter possess hair-like pseudopods several time longer than the spicules observed here.

Supplementary criteria: None.

Remarks: As shown for the second image of **Aulacanthidae ‘star’**, these forms can be found in pairs of two specimens.

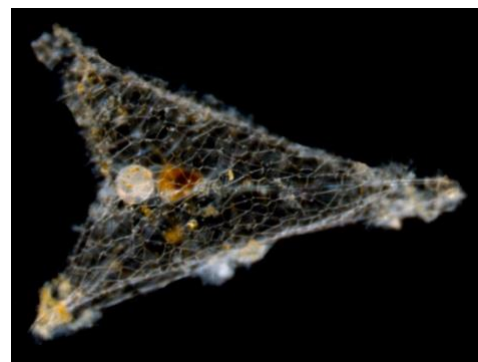
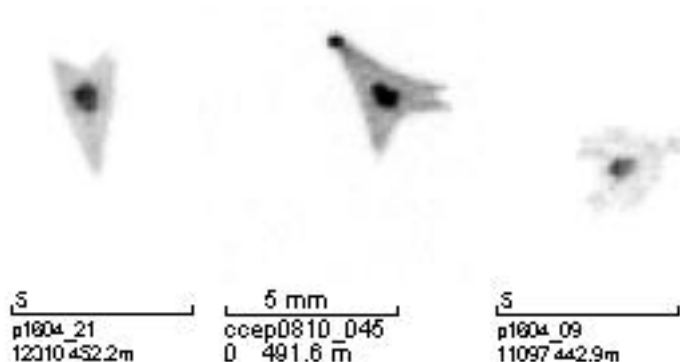
9. Coelodendridae

Four main morphotypes (not necessarily linked to specific taxa) can be distinguished among the Coelodendridae:

- Coelodendridae ‘arrow’
- Coelodendridae ‘spiky’
- Coelodendridae ‘star’
- Coelodendridae ‘leg’

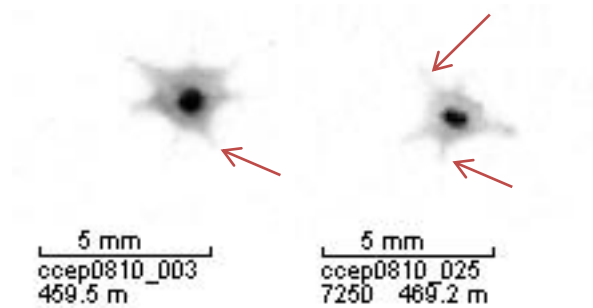
Identification (general): Like any other phaeodarian cell, all Coelodendridae possess a dark structure (phaeodium), usually located near the center of the specimen.

Coelodendridae ‘arrow’



Identification (key element): This category is characterized by an arrow-like shape. The complexity of the ‘arrow’ change from one specimen to another (e.g., 3 or 4 tips, spiky periphery)

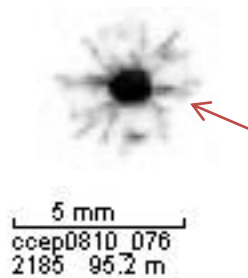
Coelodendridae ‘spiky’



Identification (key element):

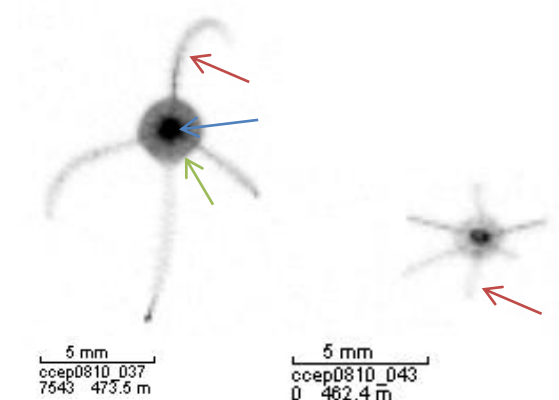
This category has an overall morphology similar to the ‘arrow’ organisms. Yet, specimens are characterized by small **projections** located at each tips of the cell. The number of projections varies from 5 to >7.

Coelodendridae ‘star’



Identification (key element): This category is characterized by a large central dark sphere from which arise **branch-like projections**. The projections divide in a binary manner from the center to the periphery of the specimen.

Coelodendridae ‘leg’



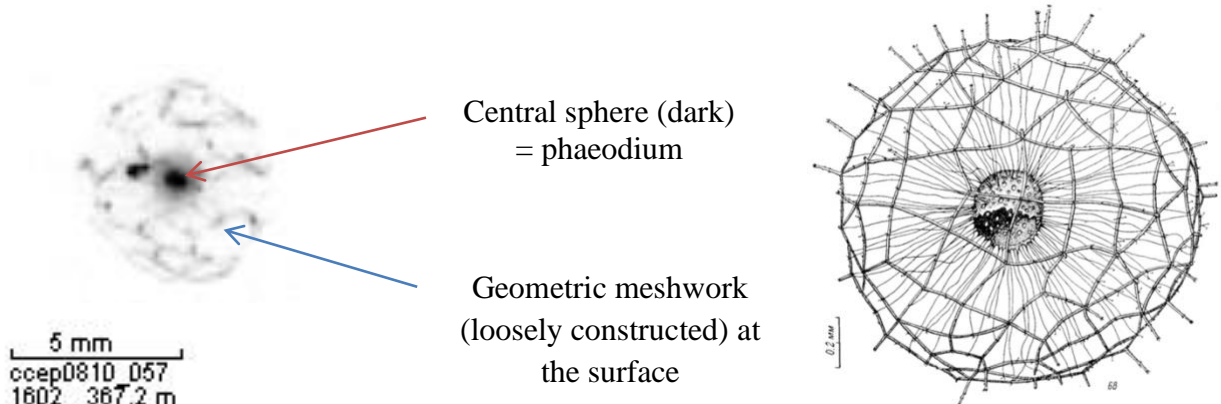
Identification (key element):

Coelodendridae with ‘legs’ are characterized by the presence of **large branch-like extensions (styles)** arising from a **central sphere** (where the **phaeodium** is located). The number of styles varies from 4 to 6 in most cases.

Confusion with other categories: Possible confusion with **Foraminifera** or **Aulosphaeridae** as described previously.

Supplementary criteria: None.

10. Cannosphaeridae



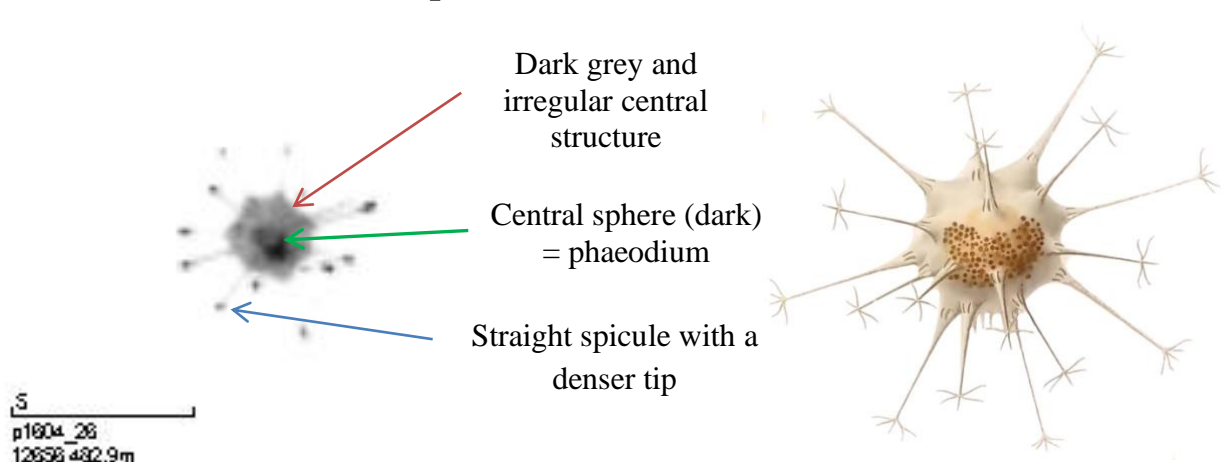
Identification: **Cannosphaeridae** are observed as large sphere with a **loosely constructed geometric meshwork** (skeleton) at the surface, and, in its center, a clearly visible **phaeodium**.

Confusion with other categories: Possible confusion with **solitary collodarians** or **Aulosphaeridae** as described previously.

Supplementary criteria: None.

Remarks: **Cannosphaeridae** can be found as pairs or colonies of several individual specimens, as shown in Figure 1.j (images with depths = 413, 354, or 414 m).

11. Phaeodaria (Circoporidae?)



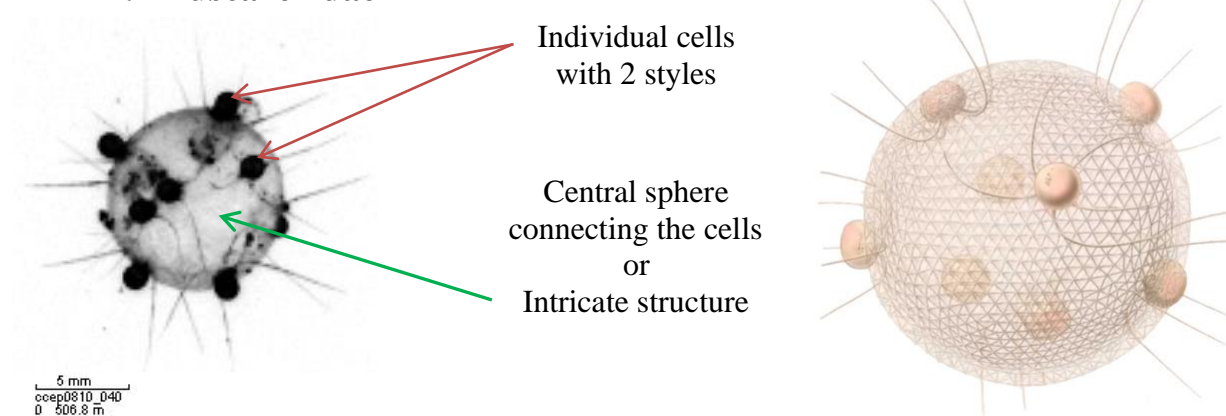
Identification: **Phaeodaria (Circoporidae?)** have a very consistent morphology composed of a **central irregular structure** (dark grey) with a **phaeodium** in its center, and multiple (11-14) **straight spicules** of medium size covering the periphery. The **tips of the spicules** are usually observed darker and denser.

Confusion with other categories: Possible confusion with **Acantharia**. Symmetry can often be seen between two opposed spicules but should not be considered as a key trait for acantharians unless the symmetry is for all spicules. Also, until now, all images of **Phaeodaria (Circoporidae?)** have been taken in deep waters (>400 m), an unlikely environment for acantharians (see explanation above).

Supplementary criteria: None.

Remarks: None.

12. Tuscaroridae



Identification: **Tuscaroridae** are almost exclusively observed as colonies composed of a dozen **individual cells**. Each individual has a visible pair of extensions (styles) orientated outward. The individual cells are attached to a **large spherical structure or a large intricate central structure**.

Confusion with other categories: None.

Supplementary criteria: None.

Remarks: **Tuscaroridae** can also be found as individual specimen (specimens observed during recent process cruises of the CCE-LTER program).

Supplementary Figures and Tables

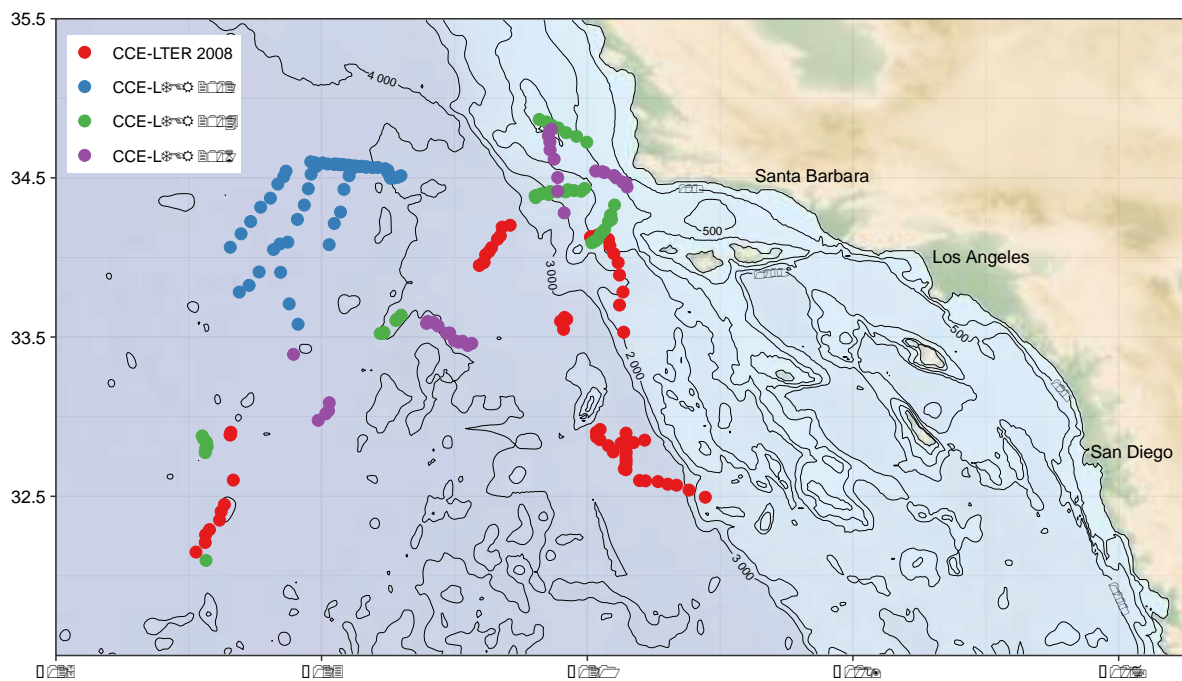


Figure S1. Location of UVP5 vertical profiles from four CCE-LTER Process cruises (colors) off the Southern California Coast.

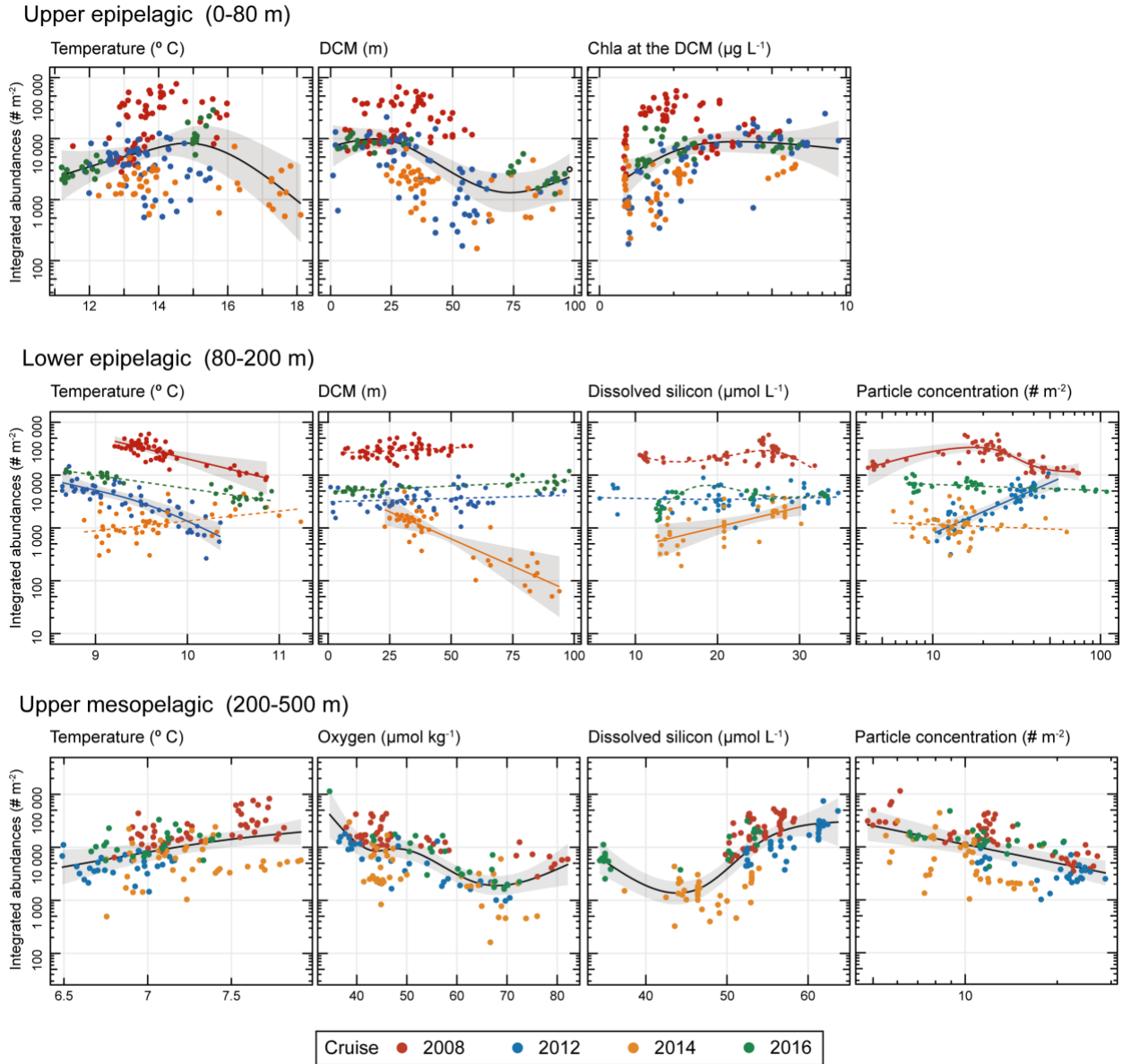


Figure S2. GAMs based on selected niche characteristics of rhizarians in the three vertical layers defined in this study. Solid lines represent significant GAMs and dashed lines, insignificant GAMs. Grey intervals denote the 95% confidence intervals for each spline.

Supplementary Table 1. Statistics for the different types of Generalized Additive Models (GAMs)

Group		Approximate significance of smoother terms (F statistic) † <i>Individual contribution of each variable running the models separately</i>						Overall model statistics			
		DCM	Chl <i>a</i> at DCM‡	Temperature	LPM‡	Oxygen	Silicic acid	R ₂ adj	Deviance explained (%)	REML	n
Epipelagic layer (0-80 m)											
Overall population		6.91 *** 16.7%	3.59 * 18.2%	5.72 *** 16.8%	--	--	--	0.49	51	153.39	193
Acantharia		n.s.	5.31 *** 25.6%	10.35 *** 19.2%	--	--	--	0.42	44.8	58.02	131
Collodaria		7.32 *** 6.9%	9.31** 9.9%	5.5** 7.2%	--	--	--	0.21	24.6	23.66	139
Lower epipelagic layer (80-200 m) ††											
Overall population	2008	n.s.	--	11.53 ** 35.1%	22.18 *** 25.2%	--	5.79 ** 33.6%	0.93††	94.2††	-34.69††	193
	2012	n.s.	--	24.79 *** 46%	74.95 *** 43.9%	--	n.s.				
	2014	20.56 *** 40.8%	--	n.s.	n.s.	--	16.05 *** 42.6%				
	2016	n.s.	--	7.45* 48.7%	n.s.	--	6.86 *** 39.8%				
Aulosphaeridae	2008	n.s.	--	11.84 *** 25.9%	7.41 ** 32.4%	--	4.54 ** 29.8%	0.91††	93.1††	-24.41††	175
	2012	n.s.	--	6.18 ** 29.4%	95.14 *** 25.6%	--	4.46 * 33.5%				
	2014	6.97 ** 33.7%	--	n.s.	n.s.	--	8.17 ** 26.6%				
	2016	n.s.	--	n.s.	n.s.	--	n.s.				
Castanellidae	2008	n.s.	--	3.47 ** 42.3%	n.s.	--	7.11 *** 12.7%	0.71††	76.4††	3.34††	149
	2012	n.s.	--	n.s.	n.s.	--	n.s.				
	2014	n.s.	--	4.36 *	n.s.	--	n.s.				
	2016	n.s.	--	16.65 *** 15.4%	5.31 ** 22.4%	--	6.02 * 20.8%				

Upper mesopelagic layer (200-500 m)									
Overall population	--	--	6.37 ** 16.34%	16.69 *** 14.31%	9.63 *** 12.35%	24.43 *** 17.29%	0.63	65.3	76.93 147
Aulacanthidae	--	--	n.s.	n.s.	n.s.	18.56 ***	0.12	12.8	25.72 129
Foraminifera	--	--	n.s.	n.s.	7.62 **	--	0.08	8.8	20.14 81
Phaeodaria (Circoporidae?)	--	--	6.56 * 44.6%	n.s.	n.s.	12.24 *** 4.2%	0.44	48.8	-7.15 43
Coelodendridae (0-250 m)	--	--	4.95 **	n.s.	n.s.	n.s.	0.26	31.1	3.72 44
Coelodendridae (250-500 m)	--	--	n.s.	n.s.	n.s.	13.71 ***	0.14	15.5	4.357 77

† Significance codes for p values: $p < 0.001$ ***; $p < 0.01$ **, $p < 0.05$ *; $p \geq 0.05$ 'n.s.'

†† For GAMs on a yearly basis (see Methods), the individual contribution of each variable is reported running the models for each year separately. The approximate significance of smoother terms (F statistics) and overall model statistics are those of the full GAM model, containing all four years together.

‡ Values are log transformed

Supplementary Table 2. Integrated abundances (#.m⁻²; mean \pm standard error of the mean) of test-bearing rhizarians in four different cruises.

Year	Site	Collodaria (0-300m)	Acantharia (0-300m)	Castanellidae (0-300m)	Aulosphaeridae (0-300m)	Rhizaria (unknown) (0-500m)	Medusetidae (0-500m)	Coelodendridae (0-250m)	Coelodendridae (0-250m)	Foraminifera (0-500m)	Cannosphaeridae (0-500m)	Aulacanthidae (0-500m)	Phacodaria (unknown)
2008	C1	319 \pm 99	560 \pm 100	1044 \pm 150	41028 \pm 5387	255 \pm 107	165 \pm 23	226 \pm 68	210 \pm 50	578 \pm 67	165 \pm 92	778 \pm 116	123 \pm 19
	C2	286 \pm 37	148 \pm 27	487 \pm 149	4860 \pm 719	161 \pm 49	-	127 \pm 20	338 \pm 43	222 \pm 25	108	854 \pm 73	298
	C3	248 \pm 29	585 \pm 89	1108 \pm 142	33515 \pm 1929	248 \pm 36	302 \pm 140	350 \pm 55	252 \pm 32	462 \pm 63	110	739 \pm 137	116 \pm 12
	C4	149 \pm 26	297 \pm 79	401 \pm 82	12479 \pm 956	201 \pm 113	206 \pm 55	160 \pm 8	299 \pm 80	310 \pm 80	199 \pm 22	528 \pm 159	206 \pm 19
	C5	182 \pm 27	129 \pm 23	277 \pm 58	7719 \pm 775	153 \pm 22	-	243	306 \pm 59	233 \pm 98	124	720 \pm 117	193 \pm 35
	C6	147 \pm 72	264 \pm 43	926 \pm 149	19040 \pm 1293	113 \pm 25	-	169 \pm 44	265 \pm 59	237 \pm 63	-	421 \pm 114	192 \pm 15
	F1	294 \pm 51	219 \pm 14	777 \pm 150	16023 \pm 2255	-	-	348 \pm 61	549	292	-	1003	211
2012	C1	215 \pm 20	1075 \pm 154	274 \pm 31	6474 \pm 336	353 \pm 115	-	194 \pm 4	452	341 \pm 86	-	876 \pm 271	187
	C2	201 \pm 69	136 \pm 52	269 \pm 62	624 \pm 217	224 \pm 67	-	-	359 \pm 85	333 \pm 59	249	759 \pm 127	264 \pm 57
	C3	158 \pm 38	403 \pm 85	284 \pm 40	6662 \pm 646	115 \pm 20	243	147	287 \pm 83	349 \pm 99	167	898 \pm 144	215 \pm 26
	C4	170 \pm 40	88	190 \pm 33	169 \pm 13	143	-	-	205 \pm 87	135	-	632 \pm 125	138 \pm 7
	C5	157 \pm 45	1038 \pm 149	169 \pm 37	952 \pm 142	351 \pm 120	180	-	570	441	139	732 \pm 162	322 \pm 111
	F1	164 \pm 24	551 \pm 129	355 \pm 63	4334 \pm 632	-	-	231	-	-	-	-	-
	F2	271 \pm 57	3551 \pm 1286	419 \pm 63	2216 \pm 566	-	-	-	-	-	-	-	-
2014	C1	299 \pm 25	816 \pm 78	226 \pm 90	388 \pm 139	266	-	-	-	111	-	244	104
	C2	334 \pm 61	714 \pm 88	184 \pm 45	1348 \pm 94	117 \pm 13	116 \pm 0	102	209 \pm 45	183 \pm 35	-	315 \pm 57	111
	C3	358 \pm 237	162 \pm 29	132 \pm 19	706 \pm 138	155 \pm 25	65	-	152 \pm 26	170 \pm 27	113	399 \pm 57	113 \pm 0
	C4	116 \pm 33	-	76	-	-	-	-	-	104	-	113 \pm 2	-
	C5	171 \pm 66	57 \pm 1	67	166 \pm 35	115 \pm 35	-	-	146 \pm 30	-	-	296 \pm 50	109
2016	C1	91 \pm 26	51 \pm 12	55 \pm 11	3180 \pm 211	49 \pm 15	83	84	100 \pm 22	85 \pm 23	74	330 \pm 60	80 \pm 32
	C2	106 \pm 15	95 \pm 30	138 \pm 29	1349 \pm 112	78 \pm 11	-	81 \pm 1	100 \pm 14	163 \pm 64	91 \pm 27	271 \pm 64	70 \pm 8
	C3	78 \pm 12	474 \pm 54	208 \pm 30	4626 \pm 274	52 \pm 8	84	130 \pm 60	119 \pm 29	68 \pm 3	79	555 \pm 82	56 \pm 7
	C4	97 \pm 19	68 \pm 15	222 \pm 52	4355 \pm 359	245	-	115 \pm 36	101 \pm 38	177 \pm 30	66	508 \pm 215	-